





 B first author 1984-2005 Bader Bilginsoy Blatz Brazzle Brostrom Brynda Hlady Gregonis Van Wagenen Davies Coleman

[View](#) [Arrange By](#) [Action](#) [Share](#) [Edit Tags](#)

Name	^	Date Modified	Size	Kind
 Bader 1984 Concanavalin A Monolayers Van Wagenen Ringsdorf.pdf		Oct 11, 2006, 5:48 PM	936 KB	PDF D
 Bilginsoy 2005 Waitzman Living With Phenylketonuria Perspectives Leonard Ernst.pdf		Oct 28, 2018, 2:54 PM	135 KB	PDF D
 Blatz, Ma 1979 Deformable Surface Theory Contact Angle unpublished.pdf		Nov 11, 2018, 2:10 PM	3.8 MB	PDF D
 Brazzle 2000 Bartholomeusz Davies Frazier Van Wagenen microneedles.pdf		Nov 10, 2018, 10:10 AM	2.1 MB	PDF D
 Brostrom 1980 Thermal Analysis Polymers Coleman Gregonis.pdf		Oct 10, 2006, 9:30 PM	505 KB	PDF D
 Brynda 1990 Protein Adsorption Energy Transfer Hlady.pdf		Oct 10, 2006, 9:24 PM	1.4 MB	PDF D

## Interactions of Concanavalin A with Polymerized Monolayers

H. BADER,<sup>1</sup> R. VAN WAGENEN,\* J. D. ANDRADE,\* AND H. RINGSDORF

*Institut für Organische Chemie, Universität Mainz, D-6500 Mainz, Federal Republic of Germany, and*

*\*Department of Bioengineering, College of Engineering, University of Utah, Salt Lake City, Utah 84112*

Received August 15, 1983; accepted March 5, 1984

Concanavalin A (Con A) interactions with hydrophobic and hydrophilic polydiacetylene surfaces were probed by total internal reflection UV fluorescence spectroscopy (TIRF). The glycolipid polydiacetylene surfaces showed the same binding specificity with Con A as soluble or membrane-bound sugars. The TIRF technique and polymerized monolayers are useful for the study of model membrane-protein interactions.

### INTRODUCTION

Lipid monolayers attached to planar solid supports have gained considerable interest as models for the study of protein-membrane (1) and cell-membrane (2) interactions. The use of highly stable polymerized monolayers, formed by diacetylenic amphiphiles following deposition by Langmuir-Blodgett technique and UV-irradiation, has been described recently (3).

Interactions of proteins with these surfaces can be monitored by TIRF spectroscopy (4). TIRF is a new technique which utilizes total internal reflection optics to generate an interface-bound evanescent wave. By exciting at 280 nm, the intrinsic UV fluorescence (310–350 nm) of protein (due to the tryptophan moieties present) can be readily monitored. As the penetration depth of the interface-bound evanescent wave is only about 1000 Å, the majority of the signal comes from that protein within several hundred Ångströms of the interface, the majority of this coming from adsorbed or surface-bound protein. TIRF is a highly surface-sensitive technique which permits real-time adsorption-desorption studies of unlabeled proteins under well-

defined conditions. Experimental and instrumentation details are available (4, 5).

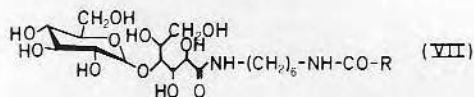
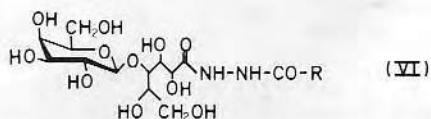
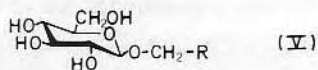
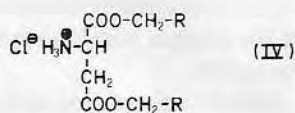
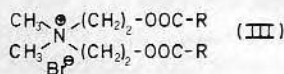
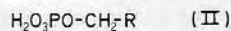
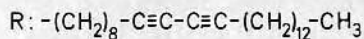
### EXPERIMENTAL

Quartz slides (Hereaus Suprasil 25 × 15 × 1 mm) were used as supports for the monolayers. The slides were cleaned (4) and silanized by dimethyldichlorosilane treatment followed by the deposition of four layers of arachidonic acid (6). A monolayer of a polymerizable diacetylenic amphiphile (Table I) was spread at the gas-water interface of a Langmuir film balance (Lauda) with water or, in the case of the long-chain carboxylic acid, 1% CdCl<sub>2</sub>-solution as the subphase. The monolayer was compressed to the solid-analog state (surface pressure: 25–40 mN/m) and the hydrophobic quartz slide was dipped through the film by means of an electronically controlled and driven dipping system. An ordered monolayer with the headgroups of the lipoids orientated toward the subphase was deposited on the first downward trip. After removal of the remaining film from the gas-water interface, the monolayer was polymerized via a UV-lamp (Hamamatsu Corp.) with an intensity of 0.5 mW/cm<sup>2</sup> for 10 min while the support was still submerged. The polymerized films appear slightly blue or red which are the typical colors of the conjugated double-triple

<sup>1</sup> To whom correspondence and reprint requests should be directed.

TABLE I

Structures of the Diacetylene Amphiphiles Used in this Work (See (9) for Details)



bond polymer backbone present in polydiacetylenes (7). A monolayer of arachidonic acid was then spread on the subphase and the slide coated with polymerized film was slowly withdrawn. The final layer of saturated carboxylic acid protects the polymerized monolayer underneath from the loss of water of hydration. This final layer can be easily removed by rinsing the slide with buffer. The monolayer assembly can be kept under ambient conditions for weeks without deterioration as evidenced by electron microscopy performed up to 3 months after the initial preparation of the monolayer.

Concanavalin A (Sigma) was dissolved in

Dulbecco's phosphate-buffered saline (PBS), pH 7.2 (8), at a concentration of 1 mg/ml, and filtered through a membrane (Schleicher & Schuell, FP030/7) prior to injection into the TIRF system. L-Tryptophan (Calbiochem, recrystallized) standards for calibration (0.02, 0.05, and 0.1 mg/ml) were prepared in the same buffer. Tryptophan fluorescence was excited at 280 nm and emission was monitored at 340 nm.

The adsorption cell and surface were rinsed and equilibrated with PBS buffer. The 1-mg/ml Con A solution was injected at a flow rate of 2.4 ml/min. Flow was stopped after 120 sec and the solution was then static for up to 120 min. Buffer was then injected at 8.8 ml/min for 270 sec to remove the protein solution and commence desorption of Con A.

Con A bound to hydrophobic dimethyldichlorosilane-treated quartz surfaces in a characteristic manner. Adsorption plateaued at 40 min. Desorption required 15 min to plateau. Typically, 86% of the protein remained irreversibly adsorbed on the hydrophobic surfaces.

On hydrophilic quartz surfaces, Con A adsorbed slowly and required more than 60 min to stabilize. Desorption occurred rapidly, leaving 53% of the protein irreversibly bound to the surface.

Table I shows the structures of the diacytlenic amphiphiles (9) investigated. Table II summarized the TIRF results for various substrates.

The adsorption behavior of Con A on negatively charged polymeric monolayers from (I) and (II) is very similar in the initial stage with a slow but steady increase in fluorescence intensity which levels off after about 60 min on surfaces from (I). On surfaces comprised of the amphiphile (II) the adsorption process still continues after 120 min which might be due to ion-exchange interactions between the strongly negative phosphate group and the lectin. Desorption on these negatively charged surfaces takes place primarily during the injection period (85% of the desorbing protein is removed during the first 50 sec) and reaches

TABLE II

Average Normalized Fluorescence Intensities			
Surface	$\bar{I}$ after adsorption	$\bar{I}$ after desorption	% Remaining on surface
Hydrophobic quartz	85,000	73,000	86
Hydrophilic quartz	26,500	14,000	53
Compound			
(I)	22,400	14,500	65
(II)	25,000	13,200	53
(III)	17,300	11,400	66
(IV)	7,700	2,500	32
(V)	11,800	4,300	36
(VI)	6,200	900	15
(VII)	14,600	9,000	62

a plateau after about 15 min with 65% of the lectin irreversibly bound to the carboxylic acid headgroups of (I) and 53% to the phosphate headgroups of (II).

The interactions of Con A with the positively charged quaternary ammonium head-group of (III) are considerably weaker with correspondingly lower fluorescence intensities than in the case of (I) and (II). The adsorption process does not attain equilibrium until after 120 min, presumably due to ion-ion interactions between protein and surface. Flushing the system with buffer resulted in 66% of the lectin tightly attached to the polar ammonium groups of (III) after desorption.

The aspartic acid ester (IV), with its weakly positive amino headgroup, proves to be a very weak substrate for Con A adsorption. The fluorescence intensities observed are only about one-third of those in the previous experiments. Only 32% of the protein remains on this surface after desorption.

The polymerizable glycolipids with their  $\beta$ -glucopyranose ( $\beta$ -Glcp) (V),  $\beta$ -galactopyranose ( $\beta$ -Galp) (VI), and  $\alpha$ -glucopyranose ( $\alpha$ -Glcp)

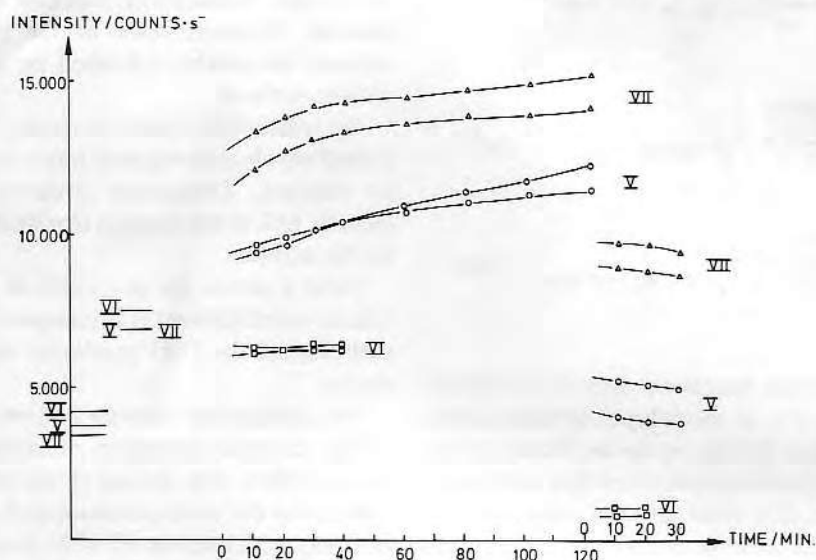


FIG. 1. Adsorption of Con A on different polymerized glycolipid monolayers. The vertical axis is normalized fluorescence intensity. The horizontal axis is time in minutes. At the far left the intensities of the tryptophan standards are indicated for the various experiments. The numbers vary slightly because each experiment requires a different assembly of the quartz prism-plate combination; small amounts of scattering produce a signal from the bulk solution. This signal is removed from the total by the normalization and quantization procedures (5). Time zero is indicated as that time from which the rapid injection begins. The solution enters the center of the cell sampling volume within 2 sec. Time zero at the far right is that time at which the desorption sequence begins, wherein the protein solution in the cell is flushed out by buffer. The adsorbed protein concentration is monitored with time, i.e., the desorption kinetics. The numbers refer to the compounds in Table I.



(VII) headgroups are of particular interest in their different interactions with the  $\alpha$ -Manp- and  $\alpha$ -Glc-p-specific Con A (Fig. 1 and Table II). In agglutination experiments with glycolipid-bearing liposomes, no recognition and binding of Con A to  $\beta$ -Galp headgroups were observed (10). Our TIRF experiments demonstrate that there was little interaction between polymerized monolayers of glycolipid (VI) and Con A. Fluorescence intensities stabilize during the injection period and no further increase can be detected over a 40-min time interval. Only 15% of the protein remains on these surfaces after desorption, presumably due to weak polar forces between the protein and the sugar moieties.

Polymerized vesicles from (V) were agglutinated by Con A (11) indicating the possibility of lectin-sugar interactions if the sugar moieties are presented in high area density. Indeed, a substantial adsorption of Con A on polymerized monolayers of the  $\beta$ -Glc-p glycolipid (V) was observed which takes more than 120 min to reach plateau. Flushing buffer through the system removes protein fluorescence rapidly; 36% of the lectin remains attached to the surface after desorption.

The polymerizable  $\alpha$ -Glc-p glycolipid (VII) with the sugar headgroup in proper configuration to be recognized by Con A interacts strongly with the lectin when orientated in polymerized hydrophilic monolayers; 62% of the protein is bound irreversibly to the surface.

#### CONCLUSIONS

Our results indicate that the lectin concanavalin A interacts very strongly with hydrophobic surfaces. Hydrophilic surfaces comprised of the negatively charged headgroups of diacetylenic lipoids organized in polymerized monolayers bind this protein to a larger extent than positively charged films on a planar solid support. The adsorption of Con A to the sugar headgroups of glycolipids in polymerized monolayers is dependent on the

configuration of the glycopyranose moieties with little binding to  $\beta$ -Galp, more binding to  $\beta$ -Glc-p, and even more adsorption to  $\alpha$ -Glc-p.

Stable polymerized monolayers with the hydrophilic headgroups of the amphiles orientated to the aqueous environment were shown to be useful tools for the study of protein-membrane interactions. The deposition of lipid monolayers on hydrophobic planar supports and the stabilization of these surfaces by polymerization results in model surfaces useful for a variety of fundamental surface chemical and protein adsorption studies.

#### ACKNOWLEDGMENTS

We thank Suzanne Winters and Monty Reichert for many valuable contributions during the course of this investigation. This work was partially supported by NIH Grant HL 18519.

#### REFERENCES

1. Hafeman, D. G., Tscherner, V., and McConnell, H. M., *Proc. Nat. Acad. Sci. USA* **78**, 4552 (1981).
2. Weis, R. M., Balakrishnan, K., Smith, B. A., and McConnell, H. M., *J. Biol. Chem.* **257**, 6440 (1982).
3. Albrecht, O., Johnston, D. S., Villaverde, C., and Chapman, D., *Biochim. Biophys. Acta* **687**, 165 (1982).
4. Van Wagenen, R., Rockhold, S., and Andrade, J. D., in "Biomaterials" (S. L. Cooper and N. A. Peppas, Eds.), Vol. 199, pp. 351-370. Adv. Chem. Ser., Amer. Chem. Soc., Washington, D. C., 1982.
5. Rockhold, S., Quinn, R., Van Wagenen, R., Andrade, J. D., and Reichert, W. M. *J. Electroanal. Chem.* **150**, 261 (1983).
6. Bucher, H., V. Elsner, O., Mobius, D., Tillman, P., and Weigand, J., *Z. Phys. Chem.* **65**, 152 (1969).
7. Lopez, E., O'Brien, D. F., and Whitesides, T. H., *J. Amer. Chem. Soc.* **104**, 305 (1982).
8. Dulbecco, R., and Vogt, M., *J. Exp. Med.* **99**, 167 (1954).
9. Gros, L., Ringsdorf, H., and Schupp, H., *Angew. Chem.* **93**, 311 (1981); *Angew. Chem. Int. Ed. Engl.* **20**, 305 (1981).
10. Goldstein, I. J., in "Advances in Experimental Medicine and Biology" (T. K. Chowdhury and A. K. Weiss, Eds.), Vol. 55, pp. 35-53. Plenum, New York, 1975.
11. Bader, H., Ringsdorf, H., and Skura, J., *Angew. Chem.* **93**, 109 (1981); *Angew. Chem. Int. Ed. Engl.* **20**, 90 (1981).

## Living with phenylketonuria: Perspectives of patients and their families

C. BILGINSOY<sup>1\*</sup>, N. WAITZMAN<sup>1</sup>, C. O. LEONARD<sup>2</sup> and S. L. ERNST<sup>2</sup>

<sup>1</sup>*Department of Economics,* <sup>2</sup>*Department of Pediatrics, University of Utah, Salt Lake City, Utah, USA*

*\*Correspondence: University of Utah, Department of Economics, 1645 Central Campus Dr., Room 308, Salt Lake City, UT 84112, USA. E-mail: bilginsoy@economics.utah.edu*

*MS received 22.03.04 Accepted 03.10.04*

**Summary:** This study surveyed PKU patients and their primary caretakers to assess their current management practices, the barriers to effective management, and the potential utility of a home monitor in managing PKU. A survey instrument was mailed to caretakers of all 50 patients with PKU in Utah between the ages of 2 and 18 years in 1997 (response rate 64%). It included separate components for caretakers and patients aged 10 to 18 years. Although there was uneven compliance with recommended practices, caretakers universally recognized the negative consequences of not adhering to the low-protein diet. There was, however, disagreement regarding such consequences among the older children surveyed. The primary obstacles cited to better adherence were time constraints and stress associated with food preparation and record-keeping, and the restrictions imposed on social life. Phenylalanine test results were regarded as the principal signal for the need for dietary adjustment. Despite the facts that obstacles to dietary adherence are multifaceted and that no single intervention would therefore serve as a panacea, a large majority of respondents believed a home monitor would facilitate better management of PKU through more regular and timely feedback.

Phenylketonuria (PKU) is an inborn metabolic disorder caused by phenylalanine hydroxylase deficiency, which, if not diagnosed and treated at birth, causes severe irreversible mental retardation. There is a nationwide newborn screening in the United States for this condition. Treatment requires maintenance of therapeutic blood phenylalanine (Phe) levels through a low-Phe diet. Diets must be individualized and periodically adjusted to maintain adequate nutrition for physical development. A synthetic protein source (formula) is required to provide adequate nutrition intake. Several studies have shown that discontinuation of the diet results, over time, in neuropsychological and behavioural problems as well as decline in IQ (Koch et al 1987, 2002; NIH 2001; Pietz et al 1988; Ris et al 1994; Rylance 1989; Smith et al 1988; Wappner et al 1999; Weglage et al 1992). Health professionals generally agree that the patient must therefore adhere to the diet throughout life (Medical Research Council 1993b). Blood Phe levels of women with PKU must be strictly controlled

during childbearing age in order to prevent damage to the fetus. Currently, the protocol for monitoring of Phe levels requires periodic drawing of blood by the patient, followed by laboratory analysis of the sample and a report back to the patient, generally within a week.

Similarly to other chronic conditions such as diabetes and hypertension, successful management of PKU is dependent on patients and their families. However, the rate at which patients 'comply with' or 'adhere to' the PKU diet typically declines as they move into adolescence (Medical Research Council 1993b; NIH 2001; Weglage et al 1992). Given the potentially serious consequences of elevated blood Phe levels, it is critical to identify the obstacles to better management faced by patients and their families, and to devise policies and procedures to alleviate them.

Clinicians often cite the restrictiveness of the recommended diet, the palatability of medical foods, testing frequency, knowledge and perceived value of the diet, psychosocial problems, the cost of medical foods and formula, and the availability of professional support as factors that hinder adherence (NIH 2001; Seashore et al 1999; Wappner et al 1999). Little is known about these obstacles, however, from the perspective of patients and their parents. Four previous surveys collected information on various aspects of the management of PKU. A German study, based on narrative interviews with parents of 8-year old PKU patients ( $n = 11$ ), found that parents did not follow a strict dietary regimen but compromised between the dietary recommendations and personality development of the child (Awiszus and Unger 1990). A Minnesota study ( $n = 43$ ) focused on the effects of family functioning on the management of PKU and concluded that family cohesion and education were positively correlated with metabolic control and the patient's IQ level (Shulman et al 1991). Another study surveyed PKU clinics in the United States and Canada regarding frequency of visits, dietary control and noncompliance policies (Fisch et al 1997). The American Association of Pediatrics (AAP) Committee on Genetics surveyed parents and young adults with PKU ( $n = 1064$ ) across the United States via the *National PKU News* in its effort to develop PKU management guidelines (Wappner et al 1999). This survey provided some summary information on PKU management practices and concluded that parents supported more stringent PKU management.

The present study reports findings of a survey distributed to Utah PKU patients in 1999. In addition to systematically exploring how patients or their caretakers currently manage dietary control and Phe-level testing, this survey elicited information concerning barriers to adherence to the diet from the perspective of both caretakers and patients, and assessed the potential utility of new home monitoring technologies from their viewpoint.

## METHODS

The survey instrument was mailed in September 1999 to all 50 classic PKU patients in Utah between the ages of 2 and 18 years, and living with a parent. While the primary care-giving parent was requested to answer all questions, patients who were aged 10 years or older were also requested to answer a subset. The survey included both closed and open-ended questions that permitted the patients and caretakers to comment in more detail on certain aspects of PKU management. As an incentive to complete and return the survey, families who responded were paid a modest compensation of \$10. Patients were asked to identify

**Table 1** Sample of PKU patients by sex and age—summary statistics

	<i>Male</i>			<i>Female</i>			<i>All</i>		
	<i>Mean age (y)</i>	<i>SD age (y)</i>	<i>n</i>	<i>Mean age (y)</i>	<i>SD age (y)</i>	<i>n</i>	<i>Mean age (y)</i>	<i>SD age (y)</i>	<i>n</i>
Patients <10 years of age	4.3	2.6	9	4.5	1.9	10	4.4	2.2	19
Patients ≥ 10 years of age	12.2	2.5	6	14.4	2.5	7	13.4	3.1	13
All patients	7.5	4.9	15	8.6	5.5	17	8.1	5.2	32

themselves on the return envelope but not on the survey instrument itself. Return envelopes and survey forms were separated upon receipt, in keeping with the promise of confidentiality made to respondents. A list of respondents was kept, however, in order to assess whether findings were subject to selection bias. Subjects who did not respond were contacted again by mail after 4 weeks. By mid-December 1999, 32 subjects (64%) had responded to the survey. Table 1 summarizes the age and sex distribution of patients who responded to the survey.

If parents who were better informed and more careful about PKU management were also more likely to respond to the survey, then the results could be subject to sample selection bias. Among the 2–5 year age cohort, such bias was not a problem because only one questionnaire (out of 13) was not returned. Among children older than 5 years, where the response rate was 51%, we assessed potential selection bias by comparing responding and nonresponding subjects in terms of patients' blood test frequencies and measured Phe levels from clinic records. These records indicated that the number of Phe tests over the previous 12 months averaged 6.4 (SD = 5.1) for responding patients and 4.0 (SD = 3.4) for nonresponding patients, a difference that is significant at the 10% level (two-tailed test). On the other hand, the mean measured Phe levels were respectively 10.0 mg/dl (SD = 6.5) and 10.6 mg/dl (SD = 4.3) for the responding and nonresponding groups and this difference was not statistically significant ( $p = 0.39$ ). Thus, there is some suggestion that in the case of children older than 5 years of age the management practices of responding and nonresponding groups were significantly different, although the impact of such differences on measured Phe levels was not significantly different.

## RESULTS

### Adherence to management recommendations

Successful management of PKU requires patients and caretakers to be familiar with the prescribed diet, to track Phe and energy intake, to monitor the physical growth of the patient, and to periodically test blood Phe levels. Survey findings summarized in Table 2 show that knowledge concerning the diet was not a problem for the overwhelming majority of caretakers (91%). Low-protein foods were used extensively (78%). Some families, however,



**Table 2** Current management practices of PKU families<sup>a</sup>

	<i>Almost always</i>	<i>Often</i>	<i>Some times</i>	<i>Almost never</i>	<i>No response</i>
The prescribed diet is known	87.5	3.1	6.3	3.1	0.0
Special low-protein foods are used	50.0	28.1	15.6	6.3	0.0
A count of the amount of Phe used is kept	37.5	25.0	25.0	12.5	0.0
Adequate calories are consumed	40.6	31.3	12.5	12.5	3.1
A count of calories consumed is kept	6.3	6.3	25.0	62.5	0.0
Child's height and weight are measured	6.3	28.1	50.0	12.5	3.1
Diet records are kept before each blood level	40.6	15.6	25.0	18.8	0.0
Each Phe test is taken at around the same time of the day	53.1	25.0	15.6	6.3	0.0
Prior to a Phe test the diet is followed more carefully	9.4	37.5	34.4	18.8	0.0

<sup>a</sup>Primary caretaker responses ( $n = 32$ ). Reported figures are percentages

were more lax than others in the management practices. Phenylalanine intake was monitored 'often' or more frequently by 63% of families. Although a majority of families (72%) reported adequate energy consumption, only 13% reported that they actually kept track of energy intake 'often' or more frequently. Such a discrepancy may be explained, in part, by the fact that the calorie count was normally kept by the nutritionist. Two parents commented that this was indeed the case for them.

Since protein is required for normal development, another part of the management protocol for PKU is the periodic measurement of the patient's physical development under the low-protein diet. Measurement of physical development did not appear to be a priority for most families, with 63% of caretakers reporting doing so 'sometimes' or less frequently. There was no relationship between such measurement practices and the age of the patient.

Careful dietary record keeping is important if the diet is to be adjusted in an informal manner. More than half of caretakers reported that they kept dietary records before each blood Phe level test and a large majority (78%) did so at a same time of day in accordance with clinic recommendations.

It has been noted that patients often 'prepare' for the test by changing diet just before testing (Weglage et al 1992). Indeed, a significant number of the Utah families (47%) reported that they altered their compliance behaviour in anticipation of testing 'often' or more frequently. This suggests that measured Phe levels kept by the clinic may frequently underrepresent the typical Phe levels of patients.

In response to other questions on management practices, only 6% of children were reportedly taken off the diet for more than a month. Many parents used nonclinical markers to assess how their children are doing; 47% reported that they could tell that the child's Phe level was high just by observing the child. In accordance with the clinical literature (Smith et al 1988), the reported symptoms were typically 'irritability', 'moodiness', or 'whining'. (Throughout the paper, selected quotations from respondents' comments in open questions

are provided in italics.) Only one caretaker reported physical symptoms (*'pale complexion, eczema, bags under eyes'*). Sixteen percent of parents reported that their children had learning problems (*'speech delay', 'trouble keeping with peers in classroom', 'inability to pay attention in classroom', and 'visual and perception problems'*).

### **Barriers to adherence with the diet**

Currently, the Utah Metabolic Clinic recommends blood Phe level testing once or twice a month for patients between ages 2 and 4 years, and once a month for patients older than 4 years. Based on independent review of clinic records, nonadherence to the recommended test frequency was widespread. The average number of tests over the 12 months preceding the survey for the younger cohort was 12. Three toddlers under age 3 years who were tested just six or nine times over this period posed particular concern because of the extensive damage associated with elevated Phe levels in early life. In the older cohort, the number of tests averaged 6.6 per year, with 25% of patients tested only once in a 3-month period or less frequently in the previous year. The yearly median measured Phe levels were above the recommended level of 6 mg/dl for 9% of the 2–4 years age cohort. The corresponding figure was 70% for patients between ages 5 and 18 years. Sex differences within either age cohort, in terms of testing frequencies or blood Phe levels, were not statistically significant.

The survey attempted to assess which factors, from the families' perspective, accounted for nonadherence to the diet and recommended test frequency. As noted above, the successful management of PKU requires special foods and formula, and frequent visits to health professionals, which could pose substantial financial burdens (Awiszus and Unger 1990; Medical Research Council 1993a; Wappner et al 1999). Special formula generally constitutes the largest single component of treatment cost, ranging from \$3000 to \$5000, per year, depending upon age. Utah provided payment for low-Phe formula in the past, but this policy is subject to change.

Lack of health insurance or noncoverage of certain expenses may, therefore, constitute a barrier to effective treatment. Among Utah patient families, 45% reported that PKU was not a substantial financial burden on their household. One parent qualified the response by stating that it depended on the insurance coverage, and two parents stated that they expected the financial burden to increase as the patient got older. Table 3 summarizes the extent of insurance coverage for various services and products utilized by the PKU patients. It reports only the presence or absence of insurance for various services and does not give any information on the extent of co-payment, co-insurance or deductibles. Just 6% of patients had no insurance at the time of the survey. Modified low-protein foods were not covered by insurance policies of most families (83%), a potentially serious source of financial burden. This figure is also virtually the same as that reported by the AAP national survey (Wappner et al 1999). Forty percent of families reported that all physician visits were covered by insurance, while the rest reported that some visits were covered. At least some of nutritionist and hospital visits, laboratory tests and PKU formula were also covered for most families, but 13–23% of families did not know whether their insurance covered any of these. A larger number of families (40%) were uncertain about or unaware of the coverage of their policies for psychologist visits, social worker visits and psychological testing. These

**Table 3** Extent of insurance coverage of PKU patients<sup>a</sup>

	<i>None</i>	<i>Some</i>	<i>All</i>	<i>Don't know</i>
Physician visits	0.0	60.0	40.0	0.0
Nutritionist visits	3.3	46.7	26.7	23.3
Laboratory tests	0.0	40.0	43.3	16.7
PKU formula	6.6	46.7	33.3	13.3
Modified low-protein foods	83.3	0.0	10.0	6.7
Psychologist visits	10.0	30.0	23.3	36.7
Psychological testing	10.0	26.7	23.3	40.0
Social worker visits	0.0	36.7	23.3	40.0
Hospital visits	0.0	50.0	36.7	13.3

<sup>a</sup>Responses of 30 parents (out of the total of 32) who had some form of health insurance coverage. Reported figures are percentages

patients also met with mental health professionals and social workers significantly fewer times compared with the rest of the patients.

A separate assessment was made of the extent of total out-of-pocket medical spending on medical care (physician, nutritionist, psychologist, social worker, hospital visits, laboratory and psychological tests, formula and low-protein foods) related to PKU during the 12 months preceding the survey. The reported annual out-of-pocket spending of the insured families ranged from zero to \$2400 (mean = \$550, SD = \$595). Out-of-pocket expenses were higher, on average, for patients older than 10 years than for the younger cohort patients.

PKU diet planning and preparation is a complicated, time-consuming activity that requires knowledge of foods and recipes, and continuous measurement of ingredients (Awiszus and Unger 1990). The diet is also considered to be restrictive and comprises foods that are unpalatable (Prince et al 1997). With respect to nonfinancial problems in optimal PKU management, the instrument included a series of closed- and open-ended questions. Closed-ended questions focused specifically on the demands associated with food preparation, record keeping and Phe testing. Caretakers' and older patients' responses to these questions are provided in Table 4.

According to Table 4, there were no statistically significant differences between perceptions of parents with children younger than 10 years of age and parents with older children regarding management of PKU. The widest divergences of opinion, although statistically nonsignificant, were observed in response to statements 1 and 5. While most parents did not consider the preparation of the diet foods overly burdensome and found the Phe level testing more cumbersome, these hold true for a relatively larger number of older patient parents. These findings may be attributable to the experience of or greater involvement of patients with PKU management. Responses to other statements are more concordant. Dietary adherence required significant labour for most parents. Around 70% of parents agreed that they 'put a lot of effort into complying with the diet'. Dissatisfaction with the diet, on the other hand, was widespread. Caretakers and children who were not satisfied with the variety of foods in the PKU diet exceeded those who were satisfied by a margin of 2 to 1.

Table 4 Caretakers' and older patients' perceptions of the management of PKU<sup>a</sup>

	Caretaker with child <10 years of age <sup>b</sup>				Caretaker with child ≥10 years of age <sup>c</sup>				Child ≥10 years of age <sup>d</sup>			
	Agree	Disagree	Don't know	Don't know	Agree	Disagree	Don't know	Don't know	Agree	Disagree	Don't know	Don't know
1. Preparation of the PKU diet takes too much time and effort	38.9	50.0	10.5	0.0	25.0	75.0	0.0	0.0	23.1	50.0	12.5	12.5
2. I put a lot of effort into complying with the diet	73.7	26.3	0.0	0.0	69.2	30.8	0.0	0.0	66.7	33.3	0.0	0.0
3. I am satisfied with the variety of foods in the special diet	31.6	57.9	10.6	0.0	30.8	69.2	0.0	0.0	33.3	66.7	0.0	0.0
4. Testing the Phe level is no longer necessary at the child's current age	0.0	100.0	0.0	0.0	0.0	100.0	0.0	0.0	22.2	55.6**	22.2	22.2
5. Testing the blood Phe level is time-consuming and cumbersome	31.6	68.4	0.0	0.0	7.7	92.3	0.0	0.0	33.3	55.6*	11.1	11.1
6. It takes too long to find out the blood Phe test results	42.1	52.6	5.3	0.0	53.8	38.5	7.7	7.7	66.7	22.2	11.1	11.1
7. The wait for Phe test results makes compliance with the PKU diet difficult	31.6	63.2	5.3	0.0	30.8	53.8	15.4	15.4	44.4	22.2	33.3	33.3
8. The PKU diet would be followed more carefully if the blood Phe levels could be tested regularly at home	73.7	21.1	5.3	0.0	61.5	23.1	15.4	15.4	66.7	11.1	22.2	22.2

<sup>a</sup> Entries are percentages of responses.<sup>b</sup> *n* = 19. Number of responses: 18 to statement 1 and 19 to all other statements<sup>c</sup> *n* = 13. Number of responses: 12 to statement 1 and 13 to all other statements<sup>d</sup> *n* = 13. Number of responses: 8 to statement 1 and 9 to all other statements\* and \*\* indicate that the response of patients ≥ 10 years of age is significantly different from that of their parents (*p* < 0.05 and *p* < 0.01, respectively). None of the responses of the two groups of caretakers were statistically significantly different at *p* < 0.10

There were some notable differences between the views of caretakers and older patients concerning some aspects of the Phe testing protocol. Patients were less sure of the need for continuation of testing and more likely to be bothered by the testing protocol. Caretakers were aware of adverse consequences associated with elevated blood Phe levels and the need for a programme of sustained testing to monitor such levels. They universally believed that Phe testing at their child's current age was necessary. Older patients who were surveyed, however, were more ambivalent; a much smaller fraction (56%) of patients than their caretakers disagreed with the statement that Phe testing was still necessary at their age ( $p < 0.01$ ). They were also less likely than their parents to disagree with the statement that blood Phe level testing is time consuming or cumbersome ( $p < 0.05$ ). According to the responses to the survey, the average lag between the collection of the blood sample and obtaining test results is 5 days (range 3–10, SD = 2.2), which is shorter than the 7 day lag time observed AAP national survey (Wappner et al 1999). Patients were more likely than their parents to maintain that the waiting period was a factor that made diet compliance more difficult.

Phenylalanine testing ranked very high among families with respect to gauging the success of, and the need for, alterations in management. In their open-ended comments, provided by 84% of respondents, caretakers universally concurred that the Phe test was the primary and most important indicator of how well they were doing. Most parents (78%) indicated that they utilized the Phe test results to make adjustments in the diet. They found Phe test results useful for other reasons as well. One noted that Phe test results helped in *'work[ing] with the clinic to obtain the best results'*. Several parents reported that the Phe results gave them *'peace of mind'*. Two parents stated that Phe results were helpful in encouraging dietary compliance.

Some research has documented significant psychological and social challenges to parents in the management of PKU and the attendant struggle to find a balance between strict dietary control and flexible developmental goals for the child (Awiszus and Unger 1990), but this research has not explored how the management of PKU affected family life. When asked to comment on the overall impact of PKU on the quality of their lives, Utah parents expressed varying degrees of adjustment to living with PKU, with responses ranging from *'[it is] hell'* and *'it's a mess'* to *'positive'*. The two major sources of stress related to food planning/preparation and ramifications of the diet for social life. Difficulties in finding low-protein foods, in finding time to prepare different meals for different members of the family and in record keeping were mentioned frequently. Problems encountered in social life included the child's interaction with peers and the planning of family events such as eating out or holidays. While acknowledging the time-consuming nature of PKU management, some caretakers seemed to accept that such management was a necessary and even worthwhile part of their lives that they had integrated into their daily routine. One parent simply stated that they *'haven't let (PKU) affect our quality of life'*. Another parent was *'[now] eating healthier, more organized in planning meals and more empathic with anyone who has a disability or a medical problem'*. Maturation of the patient can have both positive and negative effects on the management of PKU. According to one parent, *'early in life I felt [management] was more difficult—but since [my child] has taken control of the diet herself I see her making wise choices and eating "normally" as a vegetarian'*.

### The utility of a new home monitoring technology

It has been suggested that providing rapid feedback with home monitoring of Phe levels would help to maintain metabolic control and increase compliance with the PKU diet (NIH 2001; Peterson et al 1988; Seashore et al 1999; Wappner et al 1999; Wendel and Langenbeck 1996). Although the majority of parents did not consider the current protocol for testing burdensome, there was a nearly uniform perception that a home monitor could make management of the condition easier and more effective. When asked about the relationship between dietary compliance and testing, the majority of caretakers and older children who responded agreed that 'the PKU diet would be followed more carefully if blood Phe levels could be tested regularly at home' (Table 4). In their open-ended comments, the underlying rationale behind these responses was made clear. Parents regarded the prospect of home testing as a tool for more efficient management. They maintained that the primary utility of the monitor resided in the immediacy of feedback, so that Phe levels could be maintained consistently through quick dietary adjustment. Parents also indicated a willingness to pay an average per test of \$7.06 (range = \$0.75–15.00, SD = \$4.37, median \$5.00). One diabetic parent stated that he or she would be willing to pay '*as much as a diabetic*'.

### DISCUSSION

Controlling ingestion of Phe is currently the only effective means to successfully manage PKU. The results of a survey of Utah PKU families reported here provide some insights into the multitude of challenges PKU families face in following the recommended low-Phe diet, particularly as patients reach adolescence.

While all Utah PKU families recognized that there were long-term negative consequences of not complying with the diet, it is not clear how detailed their understanding of these consequences was. Although no single factor emerged as dominant, the primary obstacles to successful management of PKU cited by caretakers were time constraints and stress related to preparation of the diet foods, the keeping of records, and the restrictions imposed on social life by PKU. The significant discordance between caretakers and older patients regarding the value and inconvenience of Phe level testing provides insight into the difficulties of PKU management as patients age. Given the multitude of problems, there is no a panacea to the difficulties faced by patients and caretakers in adherence to the diet. Even so, modification of Phe testing technology may have some potential to improve management. Caretakers recognized the test as the principal indicator that dietary adjustment was necessary. About two-thirds of the respondents agreed that a home-monitoring technology would be desirable. The primary attraction of such a monitor would be the timeliness of feedback that permitted the isolation of sources of Phe level changes and immediate remedial action.

These findings were elicited from families in Utah but are likely to be generalizable to the general PKU population. First, the evidence for sample bias within the Utah population is not strong. Secondly, a multivariate analysis of determinants of blood Phe levels of patients in Utah, Nevada and Montana showed that there were no statistically significant differences among the patients across these three states in terms of testing frequency and measured blood Phe levels (Waitzman et al 2004). Finally, the Utah and the AAP national survey samples exhibited certain similarities in terms of the willingness expressed to change current



practices—to adopt a new technology and to adopt more stringent diet or more frequent Phe testing (Wappner et al 1999), respectively—for more effective management of PKU. A larger sample would certainly provide more definitive results, particularly in the case of older patients as the paucity of young adolescents in the sample and their low response rate made findings concerning their views especially tentative.

In many chronic conditions like diabetes, it is increasingly accepted that better self-management requires collaboration between patient and clinician, where the responsibility of daily management of the condition resides with the patient and his or her family while the clinician supplies the necessary expertise and support (Glasgow and Anderson 1999). The expressed willingness and desire of patients and caretakers in Utah to adopt a home monitor to test Phe levels and to take a more active role in the management of PKU fits within this emerging paradigm of a less-hierarchical relationship between the patient and the clinic and a more active role for patients in managing their chronic conditions.

## ACKNOWLEDGEMENTS

This research was supported through a grant from the Whitaker Foundation via a joint programme with the National Science Foundation on Cost Reducing Health Care Technologies. The authors would like to thank Joseph Andrade, Robert Huefner, Steven Kern, Ken Smith and two anonymous reviewers for comments and suggestions.

## REFERENCES

- Awiszus D, Unger I (1990) Coping with PKU: results of narrative interviews with parents. *Eur J Pediatr* **149**: S45–51.
- Fisch RO, Matalon R, Weisberg S, Michals K (1997) Phenylketonuria: current dietary treatment practices in the United States and Canada. *J Am Coll Nutr* **16**: 147–151.
- Glasgow RE, Anderson RM (1999) In diabetes care, moving from compliance to adherence is not enough. Something entirely different is needed [letter; comment]. *Diabetes Care* **22**: 2090–2092.
- Koch R, Azen CG, Hurst N, Friedman EG, Fishler K (1987) The effects of diet discontinuation in children with phenylketonuria. *Eur J Pediatr* **146**: A12–16.
- Koch R, Burton B, Hoganson G, et al (2002) Phenylketonuria in adulthood: a collaborative study. *J Inherit Metab Dis* **25**: 333–346.
- Medical Research Council Working Party on Phenylketonuria (1993a) Phenylketonuria due to phenylalanine hydroxylase deficiency: an unfolding story. *BMJ* **306**: 115–119.
- Medical Research Council Working Party on Phenylketonuria (1993b) Recommendations on the dietary management of phenylketonuria. *Arch Dis Child* **68**: 426–427.
- NIH Consensus Development Panel (2001) National Institutes of Health consensus development conference statement. Phenylketonuria: screening and management, October 16–18, 2000. *Pediatrics* **108**: 972–982.
- Peterson K, Slover R, Gass S, Seltzer WK, McCabe LL, McCabe ER (1988) Blood phenylalanine estimation for the patient with phenylketonuria using a portable device. *Biochem Med Metab Biol* **39**: 98–104.
- Pietz J, Benninger C, Schmidt H, Scheffner D, Bickel H (1988) Long-term development of intelligence (IQ) and EEG in 34 children with phenylketonuria treated early. *Eur J Pediatr* **147**: 361–367.
- Prince AP, McMurray MP, Buist NR (1997) Treatment products and approaches for phenylketonuria: improved palatability and flexibility demonstrate safety, efficacy and acceptance in US clinical trials. *J Inherit Metab Dis* **20**: 486–498.

- Ris MD, Williams SE, Hunt MM, Berry HK, Leslie N (1994) Early-treated phenylketonuria: adult neuropsychologic outcome. *J Pediatr* **124**: 388–392.
- Rylance G (1989) Outcome of early detected and early treated phenylketonuria patients. *Postgrad Med J* **65**: S7–9.
- Seashore MR, Wappner R, Cho S, de la Cruz F (1999) Development of guidelines for treatment of children with phenylketonuria: report of a meeting at the National Institute of Child Health and Human Development held August 15, 1995, National Institutes of Health, Bethesda, Maryland. *Pediatrics* **104**: e67.
- Shulman S, Fisch RO, Zempel CE, Gadish O, Chang PN (1991) Children with phenylketonuria: the interface of family and child functioning. *J Dev Behav Pediatr* **12**: 315–321.
- Smith I, Beasley MG, Wolff OH, Ades AE (1988) Behavior disturbance in 8-year-old children with early treated phenylketonuria. Report from the MRC/DHSS Phenylketonuria Register. *J Pediatr* **112**: 403–408.
- Waitzman NJ, Bilginsoy C, Leonard CO, Ernst S, Prince A (2004) The effect of phenylalanine test frequency on management of phenylketonuria (PKU). University of Utah.
- Wappner R, Cho S, Kronmal RA, Schuett V, Seashore MR (1999) Management of phenylketonuria for optimal outcome: a review of guidelines for phenylketonuria management and a report of surveys of parents, patients, and clinic directors. *Pediatrics* **104**: e68.
- Weglage J, Funders B, Wilken B, et al (1992) Psychological and social findings in adolescents with phenylketonuria. *Eur J Pediatr* **151**: 522–525.
- Wendel U, Langenbeck (1996) Towards self-monitoring and self-treatment in phenylketonuria—way to better diet compliance. *Eur J Pediatr* **155**: S105–107.

Prof. Paul J. Blatz  
5825 Norwich Ave.  
Van Nuys, Calif. 91411  
Tel: 213-780-4701  
Sept. 6, 1979

RECEIVED

SEP 10 1979

BIOENGINEERING

Pro. Joseph Andrade  
Dept. of Bio-Engineering  
Merrill Engineering Bldg  
University of Utah  
Salt Lake City, 84112, Utah

Dear Joe

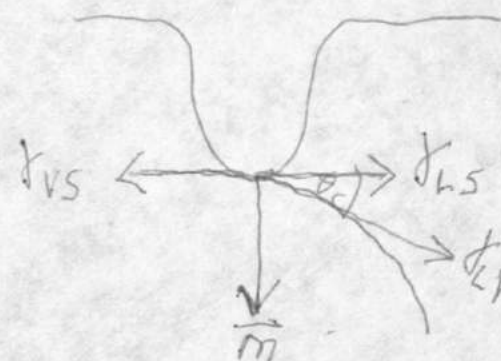
Enclosed are the refereed comments on our ill-fated paper, and below are some of my comments.

Since I talked to you on the phone a few days ago I sat and thought very intensively about the problem. It is, of course, a very facinating one. There is no doubt that the linear solution obtained by applying  $-\phi H(a-r) + \gamma_{LV} \sin \theta_c \delta(a-r)$  to a flat surface leads to an infinite displacement at  $r=a$ . But that is only true when the vector is normal to the surface. Upon thinking about it, I now realize this is only true for a flat surface. The disparity, however, does not arise, as Rusanow suggests, from surface roughness, but simply from the thermodynamics. In order to determine the scenario of bubble attachment, which means where it attaches, and how big it is, and what shape it is for a given mass of enclosed vapor, one must minimize a function which is the sum of Gibb's function for the vapor, plus the surface energy of the vapor film, plus the surface energies of the solid films in contact with the vapor and in contact with liquid, and finally, plus the strain energy of the deformed elastic body. The net result of the minimization will be the following.....

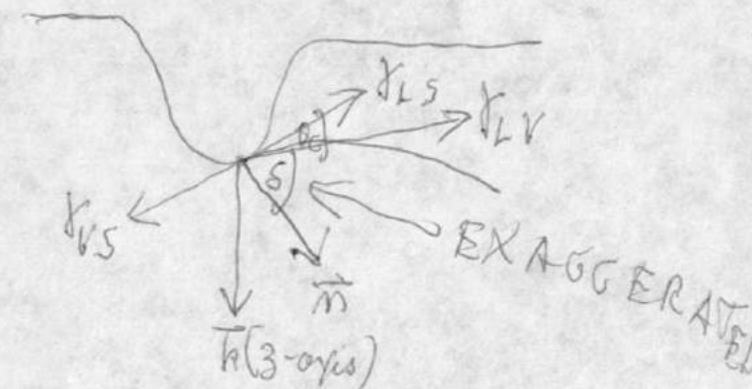
2.

The point of attachment will be such the  $\gamma_{LV} \sin \theta_c$  is not normal <sup>to the surface</sup>. The difference will add a "small" shear stress to the boundary, and, in addition, the normal component will be slightly less. If the thermodynamic contact angle on the flat surface be denoted by  $\theta_c$ , then the angle between the vector and the normal to the surface at the point of attachment will be  $(\theta_c + \delta)$ , where  $\delta$  is the extra angle between the Z-axis of the flat body and the normal to the deformed surface.

PRESENT



CORRECTED



Where, I repeat,  $\delta$ , is determined by minimizing;

$$\phi = \begin{cases} G_1 & \text{--- Gibb's Energy of VAPOR} \\ + \\ S_2 & \text{--- TOTAL Surface Energy} \\ + \\ W_3 & \text{--- Strain Energy of Gel} \end{cases}$$



Thus we do not have to do a nonlinear solution, but we do have to redo the linear elastic solution with a more general B.C. and then do the minimization. I propose to get Ma going on this if you are amenable. If you can cover a few days of my consulting time it would help me in my struggle to make a living.

Also let me suggest the following. I would to come up next Thursday, 13 Sept. 79, and lay out the thing with Ma. I would hope you could cover my traveling expenses and one day of time at \$250.00. Since Alex Oblad (His <sup>UNIV.</sup> Ext. 581-6647) is after me to finish a joint proposal on coal research, he should cover  $\frac{1}{2}$  the airfare. I will bring the proposal with me, and will stay over Friday to follow up the typing and also to double check with Ma on the work we will have done the previous day.

Please confirm my suggestions if you are amenable, ASAP.

I look forward to seeing you again.

Sincerely

*Paul*

Prof. Paul J. Blatz

# JOURNAL OF COLLOID AND INTERFACE SCIENCE

## EDITORS-IN-CHIEF

MILTON KERKER  
CLARKSON COLLEGE OF TECHNOLOGY  
POTSDAM, NEW YORK 13676

A. C. ZETTMEOYER  
BLDG. 27, ALUMNI BLDG.  
LEHIGH UNIVERSITY  
BETHLEHEM, PENNSYLVANIA 18015

## PUBLISHERS:

ACADEMIC PRESS, INC.  
111 FIFTH AVENUE  
NEW YORK, NEW YORK 10003

March 27, 1979

Dr. Shao-Mu Ma *Paul J. Blatz*  
Dept. of Engr. 3747 Clarrington Avenue #37  
University of Utah  
Salt Lake City, Utah 84112 *Los Angeles CA 90034*

Re: #5738-Z - Effect of Elastic Deformation on Contact Angles

Dear Dr. Ma"

Referee I has accepted the paper; however, Referee II finds serious errors as you will see by the attached comment sheet. We will need a suitable rebuttal to these criticisms before we can proceed.

I shall await your reply.

Sincerely

*A. C. Zettlemoyer*  
A. C. Zettlemoyer

/ewh

Return Address:

*J. Colloid and Interface Science*  
*Mrs. Coleman R. Hamel*  
*1407 W. Union Blvd.*  
*Bethlehem, Pennsylvania 18018*



Referee No. II Manuscript # 5738-Z Date 2-5-79  
 Ms Title Effect of Elastic Deformation on Contact Angles  
 Author(s) Blatz et al.

COMMENTS

It is hard to read the ms because many symbols have not been explained and mistypings have not been avoided.

Nevertheless, it is possible to make some general comments.

1. The paper deals with the theory of elasticity. There is no thermodynamics in this paper, and, consequently, the first phrase in the abstract is wrong. *← PARTLY TRUE*

2. When formulating the task, the authors postulate the surface layer thickness to be zero, so that the force applied,  $\gamma$ , acts along a line with zero area. Such a formulation means that the stress is infinite, and the strain also should be infinite in this case. That is why the zero surface layer thickness approximation has never been used in previous works. However, the authors have obtained the solution, Eq.(19), with a finite strain for this case, which is, evidently, wrong. *NOT TRUE*

Besides, the neglect of tangential stresses and strains in a solid has not been explained satisfactorily. *TRUE - AS I NOW REALIZE!*  
 Thus, both the physical formulation and the mathematical solution of the task considered are not correct.

3. The paper is closely related to recent Rusanov's theory which is actually much more general and includes, as a particular case, the task under consideration. In order to obtain the results corresponding to the formulation given in the ms, it was sufficient to put the surface layer thickness to be zero in Rusanov's formulas, from which it is very well seen that the strain becomes infinite, as it should be.

*REFERRS DOES KNOW DIFF. BETWEEN*

*STRAIN & DISPLACEMENT*

*↓  
INFINITE*

*↓  
FINITE*

*BOTH ARE COMPATIBLE*

Effect of Elastic Deformation on Contact Angles

by

Paul J. Blatz, Shao-Mu Ma\*, and Joseph D. Andrade  
 College of Engineering  
 University of Utah  
 Salt Lake City, Utah 84112

\*To whom correspondence should be addressed.



# ABSTRACT

A thermodynamic theory for calculating contact angles of deformable solids is proposed. In contrast to Rusanov's theory [1, 2] the authors do not believe that the thermodynamic contact angle given by Young's equation should differ significantly from the contact angle on a flat solid surface. For solids with Young's modulus  $\geq 10^5$  dynes/cm<sup>2</sup>, the effect of elastic deformation on the contact angle, predicted by our theory, is well within the usual experimental error ( $\pm 2^\circ$ ) and can often be ignored. For solids with Young's modulus below  $10^5$  dynes/cm<sup>2</sup> deformation becomes a significant effect. However, both our theory and Rusanov's theory should fail to apply for such materials because both theories assume linear elasticity, generally an invalid assumption for materials with moduli  $< 10^5$  dynes/cm<sup>2</sup>.

# INTRODUCTION

When a hydrophilic gel is wetted by a liquid such as water, there arises a unique distribution of surface traction which is due to the influence of the surface tension vectors. In the absence of elastic deformation, the geometry is given by Figure 1. When the drop is in thermodynamic equilibrium

$$\gamma_{1V} \cos \theta_0 = \gamma_{SV} - \gamma_{SL} \quad (1)$$

where  $\gamma_{1V}$ ,  $\gamma_{SV}$ ,  $\gamma_{SL}$  are the interfacial free energies of the liquid-vapor, solid-vapor, and solid-liquid interfaces, and  $\theta_0$  is the contact angle. The  $\gamma_{1V} \sin \theta_0$  component together with the vapor pressure of the bubble,  $\Delta P$  produces a boundary traction given by

$$\tau_{rz} = 0 \quad (2)$$

and

$$\sigma_z = -\frac{2\gamma_{1V}}{a} H(a \sin \theta_0 - R) + \gamma_{1V} \sin \theta_0 \delta(a \sin \theta_0 - R) \quad (3)$$

at the point  $z=0$  as required by static force equilibrium considerations. Here  $a$  is the radius of the bubble,  $R$  is the radius <sup>along</sup> of the wetting perimeter,  $\theta_0$  is the thermodynamic contact angle in Young's equation, and the function  $H(a \sin \theta_0 - R)$  has a value 1 for  $R < a \sin \theta_0$  and a value 0 for  $R > a \sin \theta_0$ .

Does the contact angle on the flat surface,  $\theta$ , differ significantly from the thermodynamic contact angle,  $\theta_0$ ? Is there a further change from  $\theta$  to  $\theta'$  as the surface is deformed? Rusanov [1, 2] postulated that  $\theta_0$ ,  $\theta$ , and  $\theta'$  are significantly different from one another for solids with Young's moduli less than  $10^6$  dynes/cm<sup>2</sup>, basing his analysis on the linear theory of elasticity. What actually happens could be described either by Figure 2 or by Figure 3. The vector system  $\vec{\gamma}_{1V}$ ,  $\vec{\gamma}_{SV}$ , and  $\vec{\gamma}_{SL}$  in Figure 2 rotates through a noninfinitesimal angle as deformation



occurs. Also the point of attachment of the bubble is not at the point where  $dz/dr = 0$  or at the surface,  $z = 0$ . In this case one must use nonlinear theory allowing for infinitesimal strain, but not infinitesimal rotations. Should the point of attachment of the bubble locate at the point where  $dz/dr = 0$ , as in Figure 3, then the theory of linear elasticity applies. However, we do not believe, in this case, that the value of  $\theta_0$  would differ significantly from that of  $\theta'$  for gels with Young's Modulus of the order of  $10^5$  dynes/cm<sup>2</sup>; Rusanov's theory predicts that  $\theta_0 \neq \theta'$ . Another consequence of Rusanov's refusal to identify  $\theta$  with  $\theta_0$  is the production of a shear stress on the wetted surface. He explains the ability of the surface to accomodate the stress as arising from incomplete wetting. This argument is rather poor because the contact angle itself measures the degree of wetting of a given system. With complete wetting, contact angle would be identically  $180^\circ$  for all systems. Therefore, we do not believe that  $\theta$  and  $\theta_0$  should be treated as two different quantities.

In this study a theoretical analysis of the wetting of deformable solids described by Figure 3 is given.

#### LINEAR ANALYSIS

The displacement of the point of attachment,  $\vec{u}$ , is due to the resultant force due to the pressure difference across the bubble,  $\Delta P = (P_v - P_l)$  and  $\gamma_{lv} \sin \theta'$ :

$$\vec{u} = \vec{a}_r u(r, z) + \vec{k} w(r, z) \quad (4)$$

Here, we use the actual contact angle  $\theta'$  instead of the thermodynamic contact angle  $\theta_0$ ;  $r$  and  $z$  are polar coordinates. The stress equation, in terms of the shear modulus,  $G$ , and Poisson's ratio,  $\nu$ , can be written as

$$\frac{\tau}{G} = (\nabla \vec{u} + \vec{u} \nabla) + \frac{2\nu}{1-2\nu} \nabla \cdot \vec{u} \vec{I} \quad (5)$$

in which

$$\vec{I} = \vec{a}_r \vec{a}_r + \vec{a}_\theta \vec{a}_\theta + \vec{k} \vec{k}$$

At equilibrium, the divergence of <sup>stress</sup> ~~force~~ must vanish, i.e.,

$$\nabla \cdot \vec{\tau} = 0 \quad (6)$$

In terms of dilatation,  $I_e$ , and Laplacian,  $\Delta$ , one obtains

$$\Delta \vec{u} + \frac{\nabla I_e}{1-2\nu} = 0 \quad (7)$$

Substituting the expressions for  $\vec{u}$ ,  $\nabla$ ,  $\vec{I}$ ,  $I_e$  and  $\Delta$  into equation (7), we have

$$(2 - 2\nu) \left( u_{rr} + \frac{u_r}{r} - \frac{u}{r^2} \right) + w_{rz} + (1 - 2\nu) u_{zz} = 0 \quad (8)$$

and

$$u_{rz} + \frac{u_z}{r} + (2 - 2\nu) w_{zz} + (1 - 2\nu) (w_{rr} + w_r/z) = 0 \quad (9)$$

Here, the subscripts  $r, z$  refer to the independent variables with respect to which the derivatives of  $u$  and  $w$  are taken.

Introducing the Hankel transforms [3]

$$\hat{u} = \int_0^\infty u J_1(kr) r dr \quad (10)$$

and

$$\bar{w} = \int_0^\infty w J_0(kr) r dr \quad (11)$$

Equations (8) and (9) can be written as

$$-(2 - 2\nu)k^2 \hat{u} + (1 - 2\nu) \hat{u}_{zz} - k\bar{w}_z = 0 \quad (12)$$

and

$$(2 - 2\nu) \bar{w}_{zz} + k\hat{u}_z - (1 - 2\nu) k^2 \bar{w} = 0 \quad (13)$$

where  $J_1(kr)$ ,  $J_0(kr)$  are the unmodified Bessel functions [3] of the first order and the zeroth order, respectively. The solutions of equations (12) and (13) are

$$\hat{u} = Be^{-kz} (kz - 1 + 2\nu) = Be^{-kz} kz \quad (14)$$

and

$$\bar{w} = Be^{-kz} (2 - 2\nu + kz) = Be^{-kz} (1+kz) \quad (15)$$

with

$$B = \frac{\gamma_{1v}}{G} \left[ \frac{\sin \theta' J_1(ka \sin \theta')}{k^2} - \frac{a \sin^2 \theta' J_0(ka \sin \theta')}{2k} \right] \quad (16)$$

in which  $\nu = 1/2$  was assumed.

At  $z = 0$ , the surface deflection is given by  $\hat{u}_0 = 0$  and  $\bar{w}_0 = B$ ;  $B$  is defined by (16). For these conditions,

$$\bar{w}_0 = \frac{\gamma_{1v}}{G} \int_0^\infty J_0(kr) dk \left[ \frac{\sin \theta' J_1(ka \sin \theta')}{k} - \frac{a \sin^2 \theta' J_0(ka \sin \theta')}{2} \right]$$

Evaluation of the integral leads to

$$\bar{w}_0 = \frac{2\gamma_{1v} \sin \theta'}{\pi G} \left\{ H(a \sin \theta' - r) E\left(\frac{r}{a \sin \theta'}\right) + \frac{r}{a \sin \theta'} H(r - a \sin \theta') \left[ E\left(\frac{a \sin \theta'}{r}\right) - \left(1 - \frac{a^2 \sin^2 \theta'}{r^2}\right) K\left(\frac{a \sin \theta'}{r}\right) \right] \right\}$$

$$= \frac{\gamma_{1v} a \sin^2 \theta'}{2G} \left\{ H\left(\frac{r - a \sin \theta'}{a \sin \theta'}\right) \sum_{k=0}^\infty \left(\frac{a^2 \sin^2 \theta'}{16r^2}\right)^k \left(\frac{2k}{k}\right)^2 \right. \quad (17)$$

$$\left. + H\left(\frac{a \sin \theta' - r}{a \sin \theta'}\right) \sum_{k=0}^\infty \left(\frac{r^2}{16a^2 \sin^2 \theta'}\right)^k \left(\frac{2k}{k}\right)^2 \right\}$$

where  $H(r - a \sin \theta')$  has the value of 0 when  $r < a \sin \theta'$  and the value of 1 when  $r > a \sin \theta'$ .  $E(k)$  and  $K(k)$  are elliptical functions of the 2nd and 1st kinds, respectively;  $\left(\frac{2k}{k}\right) = \frac{2k!}{(k!)^2}$ .

We notice that

$$\bar{w}_0(0) = \frac{\gamma_{1v} \sin \theta'}{2G} \quad (18)$$

$$\bar{w}_0(a \sin \theta') = \frac{2\gamma_{1v} \sin \theta'}{\pi G} \left[ 1 - \frac{\pi}{4} \sum_{k=0}^\infty \left(\frac{2k}{k}\right)^2 \left(\frac{1}{16}\right)^k \right] \quad (19)$$

$$\text{and } \bar{w}_0(\infty) = 0 \quad (20)$$

The summation  $\sum_{k=0}^\infty \left(\frac{2k}{k}\right)^2 \left(\frac{1}{16}\right)^k$  has a value of 3.14. For  $\gamma_{1v} = 72.1$  dynes/cm,  $G = 10^6$  dynes/cm<sup>2</sup> and  $\theta' = 30^\circ$ ,  $\bar{w}_0(0) \sim 0.2$  micrometers.



# THE VOLUME OF A DEFORMED BUBBLE

The volume of an undeformed bubble (Figure 1) can be expressed as

$$V_{B1} = \frac{4}{3} \pi a^3 - \left\{ \frac{2}{3} \pi a^3 (1 - \cos \theta') - \frac{1}{3} \pi (a \sin \theta')^2 (a \cos \theta') \right\} \quad (21)$$

$$= \frac{1}{3} \pi a^3 \{2 - 3 \cos \theta' - \cos^3 \theta'\}$$

For a deformed bubble, we assume the point of attachment is located at the point where  $dz/dr = 0$ , which is the basis for applying the linear theory. From Figure 3, the volume of the upper segment of the bubble is given by

$$V_{B2} = - \int_0^{a \sin \theta'} w_0 2\pi r dr$$

$$= - \int_0^{a \sin \theta'} 2\pi r dr \left\{ \frac{2\gamma_{lv} \sin \theta'}{\pi G} E\left(\frac{r}{a \sin \theta'}\right) - \frac{\gamma_{lv} a \sin^2 \theta'}{2G} \frac{1}{a \sin \theta'} \sum_{k=0}^{\infty} \left(\frac{r^2}{16a^2 \sin^2 \theta'}\right)^k \left(\frac{2k}{k}\right)^2 \right\} \quad (22)$$

since the functions  $H(a \sin \theta' - r) = 1$  and  $H(r - a \sin \theta') = 0$  in equation (17). Upon evaluation of the integral  $E\left(\frac{r}{a \sin \theta'}\right)$ , we obtain

$$V_{B2} = \frac{\gamma_{lv} a^2 \sin^3 \theta'}{G} \left\{ \frac{2}{3} + \frac{\pi}{2} \sum_{k=0}^{\infty} \left(\frac{2k}{k}\right)^2 \left(\frac{1}{16}\right)^k \frac{k}{k+1} \right\} \quad (23)$$

The volume of the lower segment of the bubble has a similar expression as the one given in equation (21) for an undeformed bubble. The total volume of a deformed bubble is, therefore

$$V_B = V_{B1} + V_{B2} \quad (24)$$

This volume is related to the mass of the vapor,  $m_v$ , by the gas law.

$$\left(P_1 + 2 \frac{\gamma_{lv}}{a}\right) V_B = \frac{m_v}{M_v} RT \quad (25)$$

where  $M_v$  is the molecular weight of the material forming the bubble. Since  $P_1 \gg \frac{2\gamma_{lv}}{a}$  and  $V_{B1} \gg V_{B2}$ , the expression (25) is not a practical formula for calculating the contact angle  $\theta'$ .

## THE CHANGE IN SURFACE DEFLECTION

In Figure 3, the maximum boss height

$$\Delta = w_0(0) - w_0(a \sin \theta')$$

$$= \frac{\gamma_{lv} \sin \theta'}{G} \left[ \frac{1}{2} - \frac{2}{\pi} + \frac{1}{2} \sum_{k=0}^{\infty} \left(\frac{2k}{k}\right)^2 \left(\frac{1}{16}\right)^k \right] \quad (26)$$

If the distance  $d$  and the radius of the bubble  $a$  can be experimentally determined, then

$$\Delta = d = a \cos \theta' - a = r \sin \theta' \quad (27)$$

where

$$r = \frac{\gamma_{lv}}{G} \left[ \frac{1}{2} - \frac{2}{\pi} + \frac{1}{2} \sum_{k=0}^{\infty} \left(\frac{2k}{k}\right)^2 \left(\frac{1}{16}\right)^k \right] \quad (28)$$

Thus,

$$\cos \theta' = \frac{a(d - a) - r[d(2a - d) + r^2]^{1/2}}{a^2(1 + r^2/a^2)} \quad (29)$$

$$= \left(\frac{d}{a} - 1\right) - \sqrt{\left(\frac{d}{a}\right) \left(2 - \frac{d}{a}\right)} \quad (r/a)$$

9  
16.4

5  
16.16 1024



If the distance  $d'$  instead of  $d$  is measured, which is usually the case, then we have

$$\Delta' = w_0^{(\infty)} - w_0 (a \sin \theta') = \frac{\gamma_{lv} \sin \theta'}{G} \left[ -\frac{2}{\pi} + \frac{1}{2} \sum_{k=0}^{\infty} \left( \frac{2k}{k} \right)^2 \left( \frac{1}{16} \right)^k \right] \quad (30)$$

or

$$\Delta' = d' - a \cos \theta' - a = \Gamma' \sin \theta' \quad (31)$$

with

$$\Gamma' = \frac{\gamma_{lv}}{G} \left[ -\frac{2}{\pi} + \frac{1}{2} \sum_{k=0}^{\infty} \left( \frac{2k}{k} \right)^2 \left( \frac{1}{16} \right)^k \right] \quad (32)$$

from which we obtain

$$\cos \theta' \approx \frac{d'}{a} - 1 - \sqrt{\left( \frac{d'}{a} \right) \left( 2 - \frac{d'}{a} \right)} (\Gamma'/a) \quad (33)$$

In equations (29) and (33), the first term on the right-hand side is the contribution from a non-deformable surface while the second term gives the correction due to elastic deformation. For water,  $\gamma_{lv} \approx 72.1$  dynes/cm, the correction factor  $\Gamma$  (or  $\Gamma'$ ) as a function of  $G$  is given in Table I. As long as we deal with materials stiffer than  $10^5$  dynes/cm<sup>2</sup>, the factor  $\Gamma$  (or  $\Gamma'$ ) is of the order of  $10^{-3}$  cm or smaller, and the second term on the right-hand side of equations (29) and (33) is considerably smaller than the first term. As a consequence, we may as well take

$$\cos \theta' \approx \frac{d}{a} - 1 \quad (\text{or } \frac{d'}{a} - 1) \quad (34)$$

For materials with  $G$  below  $10^5$  dynes/cm<sup>2</sup> the correction factor  $\Gamma$  (or  $\Gamma'$ ) becomes significant.

Some numerical values calculated from equations (29) and (33) for materials with shear modulus ranging from  $10^4$  to  $10^6$  dynes/cm<sup>2</sup> are given in Table 2. Notice that the maximum change in the contact angle referring to that of a nondeformable surface is less than  $1^\circ$  for materials with shear modulus equal or higher than  $10^5$  dynes/cm<sup>2</sup> and is less than  $2^\circ$  for materials with shear modulus of  $3.5 \times 10^4$  dynes/cm<sup>2</sup>, both of which are within the experimental error ( $\pm 2^\circ$ ) in current contact angle measuring techniques, unless very accurate methods are used [4, 5]. For materials with a shear modulus of  $10^4$  dynes/cm<sup>2</sup> or less, this change becomes quite significant; however, some calculated values of  $\cos \theta'$  are greater than unity indicating that the linear theory of elasticity fails to apply for such materials.

The last column of Table 2 gives the contact angle of materials with a Young's modulus of  $3.5 \times 10^5$  dynes/cm<sup>2</sup> (or shear modulus of  $1.17 \times 10^5$  dynes/cm<sup>2</sup>) and  $\gamma_{lv} = 72.1$  dynes/cm<sup>2</sup> calculated from Rusanov's theory [1] with  $a/\tau = 10^6$ ,  $b = 10^3$ , and  $\sigma_{sv}/\sigma_{lv} = 2$ . Notice that the changes in contact angle due to deformation calculated from our theory are, in general, smaller than those predicted by Rusanov's theory. Besides, our theory predicts that deformation causes the contact angle to change by a constant value (or almost constant for very soft materials) for contact angles other than  $0^\circ$  and  $180^\circ$  and do not change at all for  $0^\circ$  and  $180^\circ$  contact angles while Rusanov's theory predicts a periodic change and a phase shift from the thermodynamic contact angles. This difference between our theory and Rusanov's theory arises from the fact that we have ignored the thickness of the surface layer while Rusanov's theory has given the latter a major role in determining the contact angle of a deformable surface. In our theory the point of attachment of the bubble is assumed to occur at  $dz/dr = 0$  and  $\gamma_{sv}$  and  $\gamma_{sl}$  are assumed to lie horizontal and

in opposite directions.

Let us examine equation (29). If we write  $\frac{d}{a} - 1 = x$  and  $\Gamma/a = c$ , then

$$\begin{aligned}\cos \theta' &= \cos (\theta_0 + \Delta\theta') \\ &= \cos \theta_0 \cos \Delta\theta' - \sin \theta_0 \sin \Delta\theta' \\ &= x - c \sqrt{1 - x^2}\end{aligned}\quad (35)$$

In this expression  $\cos \theta_0 = x$ ,  $\sin \theta_0 = \sqrt{1 - x^2}$ . For small  $\Delta\theta'$ , we may write  $\sin \Delta\theta' \approx \frac{\Delta\theta'}{57.2957}$  and  $\cos \Delta\theta' \approx 1$ , thus

$$x - (\Delta\theta'/57.2957) \cdot \sqrt{1 - x^2} = x - c \sqrt{1 - x^2}$$

or

$$\Delta\theta' = 57.2957c = \text{constant}.\quad (36)$$

Notice that when  $G = 1 \times 10^5$  dynes/cm,  $c \sim 0.01$  and  $\Delta\theta' \approx 0.5^\circ$ . A similar expression can be reached from equation (33) by assuming  $d'/a - 1 = x$ .

In Rusanov's theory  $\gamma_{sv}$  and  $\gamma_{sl}$  form an angle other than  $180^\circ$  at the point of attachment of the bubble because of the finite thickness of the bubble wall. Since this thickness cannot be measured by any contact angle technique, we doubt it can play such an important role as proposed by Rusanov.

#### CONCLUSION

Within the framework of the theory of linear elasticity we have proposed a model to describe the effect of elastic deformation on the measured contact angle. According to this model:

- 1) The thermodynamic contact angle given in Young's equation should be identical to the contact angle of a flat solid surface.

- 2) The effect of elastic deformation on the measured contact angle is less than  $2^\circ$  for materials with Young's modulus of the order of  $\geq 10^5$  dynes/cm<sup>2</sup> (or shear modulus greater than  $3.5 \times 10^4$  dynes/cm<sup>2</sup>). This effect is considered insignificant in comparison to the experiment error which is generally about  $\pm 2^\circ$ , unless highly accurate methods are used to measure the contact angle.
- 3) The elastic deformation causes the contact angle to change by a constant value (or almost constant for very soft materials) with contact angles other than  $0^\circ$  and  $180^\circ$  and no change with  $0^\circ$  and  $180^\circ$  contact angles. This disagrees with Rusanov's theory which predicts the change to occur in a periodic fashion [1] with a phase shift from the thermodynamic contact angles.
- 4) For materials with shear moduli of the order of  $10^4$  dynes/cm<sup>2</sup>, the effect of elastic deformation is about  $5^\circ$ , which is considerably higher than the experimental error. However, a theory based on nonlinear elasticity would be more proper than the proposed model to describe such soft materials.

#### ACKNOWLEDGEMENTS

Portions of this work were supported by NIH Grant HL 16921-04. Discussions with R.N. King and correspondence with A.I. Rusanov have been helpful.



# REFERENCES

1. Rusanov, A.I., *Colloid J. USSR* (English Translation) 37, 614, 623, 629, 636, (1975).
2. Rusanov, A.I., *J. Colloid and Interface Science*, 63, 330, (1978).
3. Pearson, C.E., Ed., *Handbook of Applied Mathematics*, 353-354, (1974).
4. Neumann, A.W., *Adv. Coll. Interface Sci.*, 4, 105-191 (1974).
5. Johnson, R.E., R.H. Dettre, and D.A. Brandreth, *J. Coll. Interface Sci.* 62, 205 (1977).
6. Andrade, J.D., S.M. Ma, R.N. King, and D.E. Gregonis, submitted for publication.
7. Andrade, J.D., R.N. King, D.E. Gregonis, and D.L. Coleman, *J. Polymer Sci. Symp. C* (1979) in press.

TABLE 1

Correction factors,  $\Gamma$  and  $\Gamma'$ , for equation (29) and (33) for solids of different shear moduli,  $G^*$ .

$G$ (dynes/cm <sup>2</sup> )	$1 \times 10^4$	$1 \times 10^5$	$1 \times 10^6$
$\Gamma$ (cm)	$1.03 \times 10^{-2}$	$1.03 \times 10^{-3}$	$1.03 \times 10^{-4}$
$\Gamma'$ (cm)	$6.73 \times 10^{-3}$	$6.73 \times 10^{-4}$	$6.73 \times 10^{-5}$

\* The shear modulus,  $G$ , is  $\approx 1/3$  the Young's modulus,  $E$ .



Table 2.

## Numerical Calculations

$$(\gamma_{LV} = 72.1 \text{ dyne/cm, } a = 0.1 \text{ cm})$$

$\theta_0$ degree	$d/a$ (or $d'/a$ )	$(n')$ Eq. (29)					$(n')$ Eq. (33)					$\theta'$ [1] $1.17 \times 10^5$	$\Delta\theta'$ ( $G=1.17 \times 10^5$ )*	
		$G=10^4$	$3.5 \times 10^4$	$10^5$	$1.17 \times 10^5$	$10^6$	$10^4$	$3.5 \times 10^4$	$10^5$	$1.17 \times 10^5$	$10^6$		$E\theta$ (29)	$E\theta$ (33)
0	2	0	0	0	0	0	0	0	0	0	0	0	0	--
1	1.9998	3.8	2.3	1.6	1.6	1.2	3.2	2.0	1.5	1.4	1.2	0.6	0.4	--
5	1.9962	9.1	6.5	5.6	5.5	5.1	8.0	6.0	5.4	5.3	5.0	0.5	0.3	--
10	1.9848	14.7	11.6	10.6	10.5	10.1	13.3	11.0	10.4	10.3	10.0	0.5	0.3	-4.4
30	1.866	35.4	31.7	30.6	30.5	30.1	33.7	31.1	30.4	30.3	30.0	0.5	0.3	-4.8
60	1.5	65.7	61.7	60.6	60.5	60.1	63.8	61.1	60.4	60.3	60.0	0.5	0.3	-3.6
90	1	95.9	91.7	90.6	90.5	90.1	93.9	91.1	90.4	90.3	90.0	0.5	0.3	-1.3
120	0.5	126.0	121.7	120.6	120.5	120.1	123.9	121.1	120.4	120.3	120.0	0.5	0.3	+0.6
150	0.134	156.5	151.7	150.6	150.5	150.1	154.1	151.1	150.4	150.3	150.0	0.5	0.3	1.6
170	0.0152	**	171.9	170.6	170.5	170.1	175.2	171.2	170.4	170.3	170.0	0.5	0.3	1.7
175	0.0038	**	177.2	175.6	175.5	175.1	**	176.3	175.4	175.3	175.0	0.5	0.3	--
180	0	180	180	180	180	180	180	180	180	180	180	0	0	--

\*\* Calculated  $\cos \theta' > 1.0$ \*  $\Delta\theta' = \theta' - \theta_0$ 

## LIST OF FIGURES

- Figure 1. Schematic traction diagram for a flat solid surface in contact with a liquid and a vapor. The solid is assumed to have a sufficiently large elastic modulus that deformation is negligible. We have chosen to use the captive vapor bubble geometry because of our interest in polymer-water interfaces [6,7].
- Figure 2. Schematic traction diagram for a deformable solid surface in contact with a liquid and a vapor (finite rotation and infinitesimal strain).
- Figure 3. Schematic traction diagram for a deformable solid surface in contact with a liquid and a vapor. (Infinitesimal rotation and infinitesimal strain).

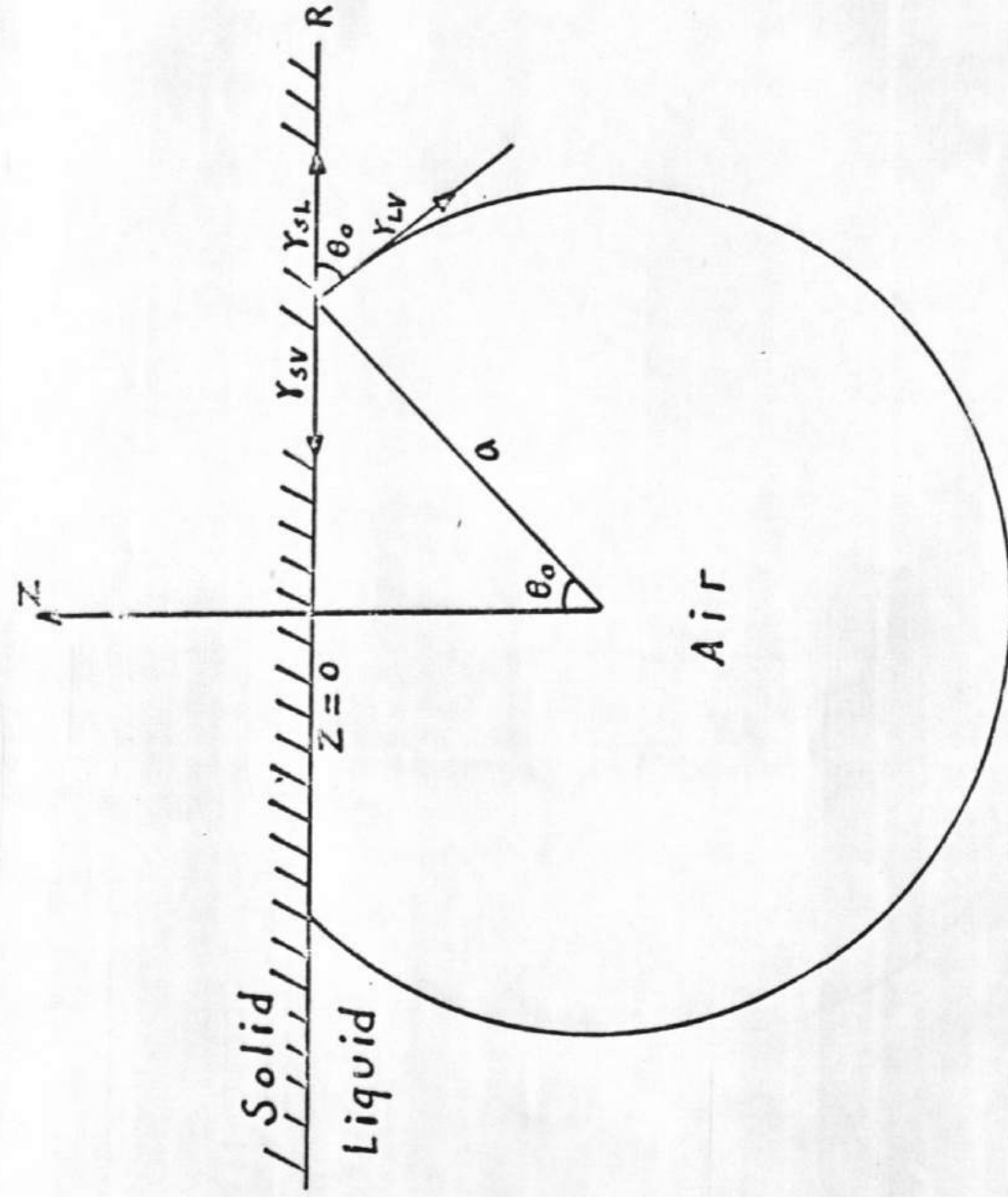


Figure 1

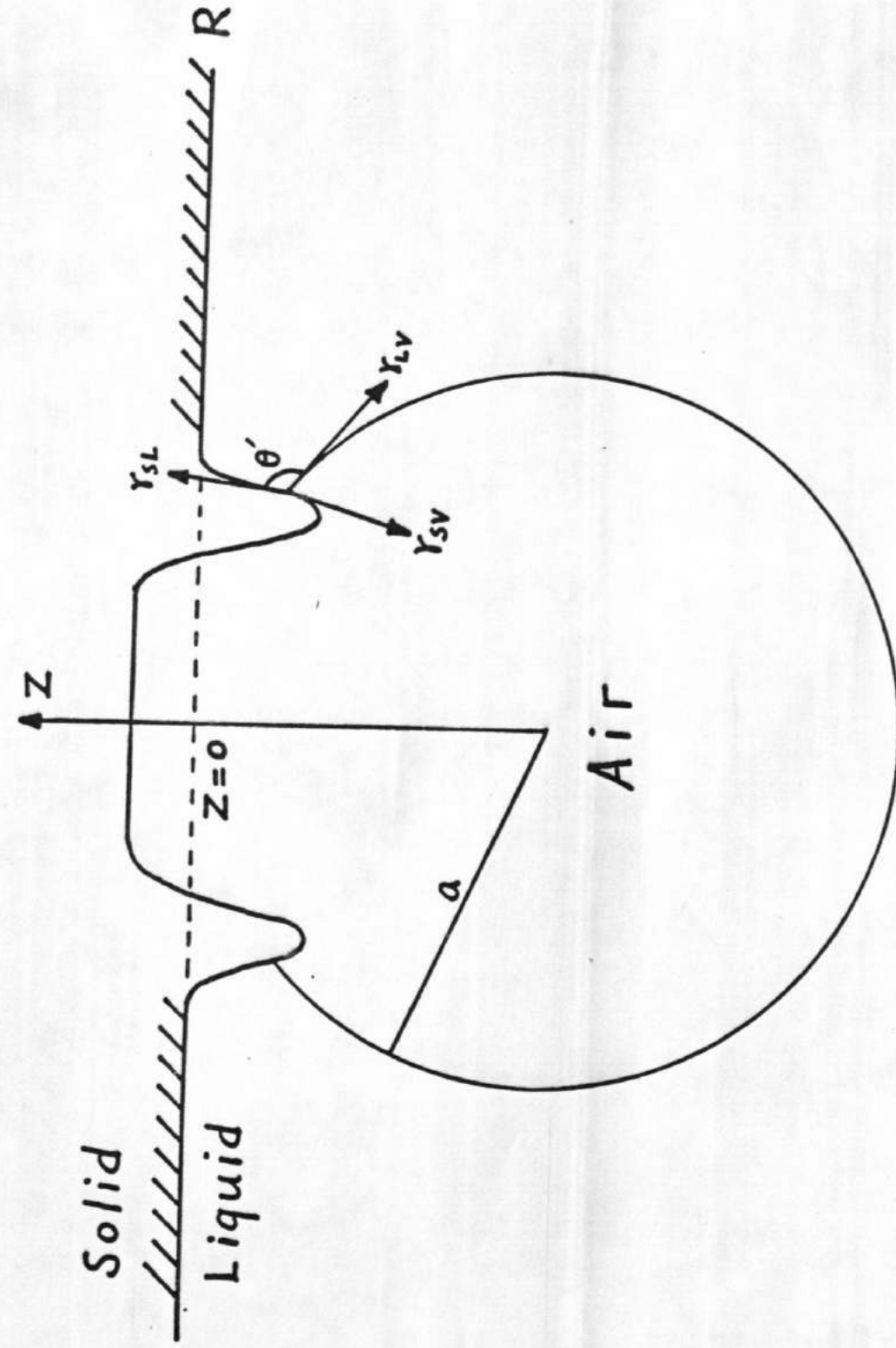
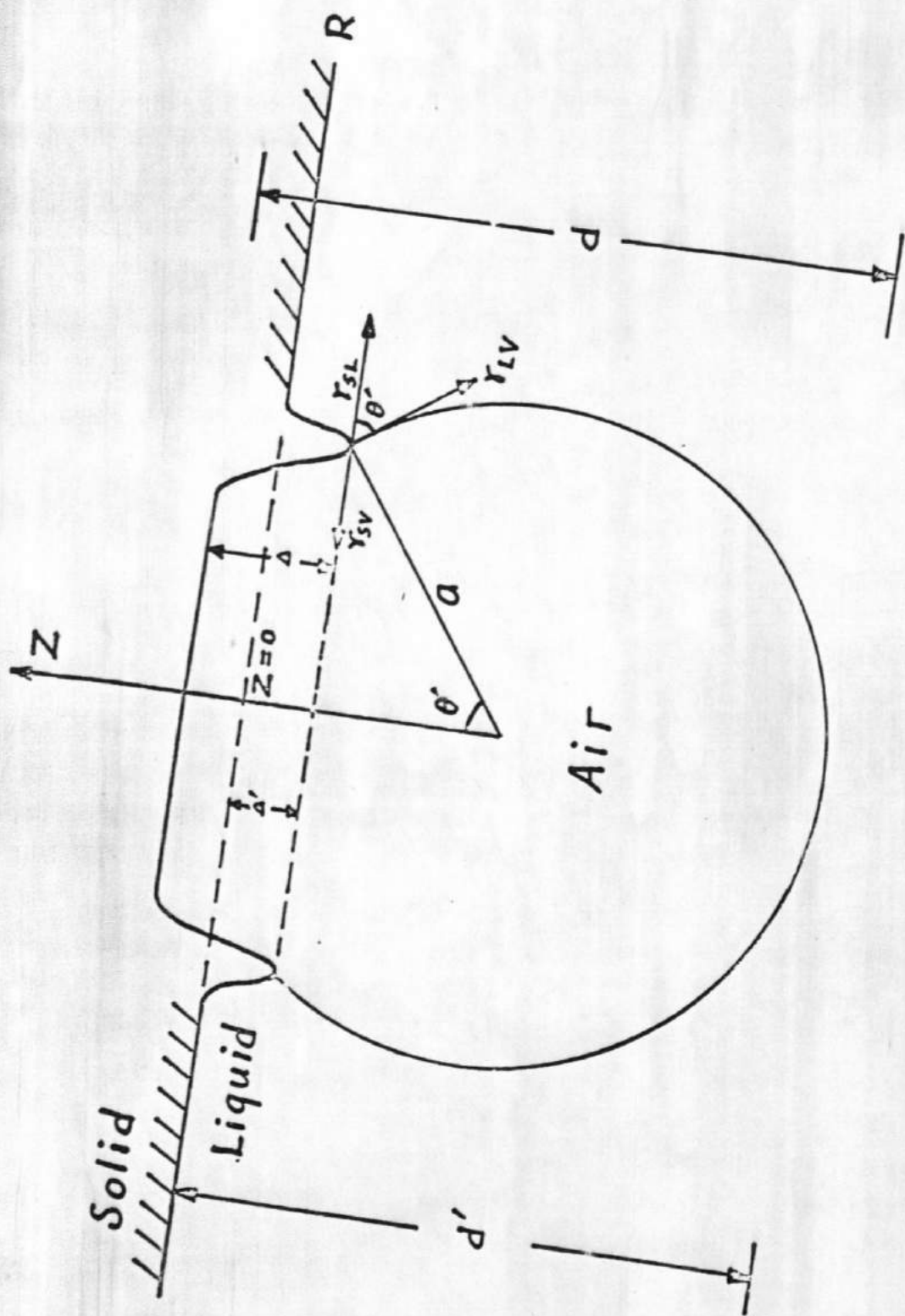


Figure 2





# ACTIVE MICRONEEDLES WITH INTEGRATED FUNCTIONALITY

John Brazzle, Dan Bartholomeusz, Rupert Davies, and Joseph Andrade

<sup>1</sup>Department of Bioengineering, University of Utah  
Salt Lake City, Utah 84112

Richard A. Van Wagenen<sup>1,2</sup>

<sup>2</sup>Protein Solutions  
Salt Lake City, Utah 84112

A. Bruno Frazier<sup>1,3</sup>

<sup>3</sup>School of ECE, Georgia Institute of Technology  
Atlanta, Georgia 30332

## ABSTRACT

The focus of this work is the design, fabrication, and characterization of a new class of biomedical micro systems, the active microneedle. Active microneedle systems represent an advancement over current microneedle technologies through the integration of additional functionality (e.g. biochemical sensing, mechanical, etc.). The active microneedles described in this paper include the following additional functionality: integration of multiple inlet/output ports, multiple lumens (flow channels), and bioluminescence based biosensors for monitoring metabolic levels (e.g. creatine and glucose).

## INTRODUCTION

Both hollow and solid microneedles and microneedle arrays have been demonstrated by a number of research groups over the past few years. Initially, only microneedles made of solid silicon had been realized [1]. Najafi and Wise developed these early microneedles that were used as neural microprobes. Recently, solid silicon microneedles fabricated by Henry et al. were formed using reactive ion etching [2]. The resulting planar needle array consisted of 20×20 needles for increasing the skin permeability to drugs. Lin, Pisano, and Muller were first to present hollow silicon processed microneedles [3,4]. These microneedles were fabricated on silicon substrate and used silicon nitride to fully enclose the channels. Later, Chen and Wise [5] presented hollow silicon microneedles for neural recording and drug delivery. These two approaches utilize a sacrificial processing technique that consumes the substrate on the devices are built. In contrast, Talbot and Pisano [6] have incorporated a polysilicon micromolding process to develop hollow microneedles. These hollow microneedles are fabricated by micromolding polysilicon (polymolding) in silicon micromolds.

Previously, we reported micromachined needles and needle arrays of hollow metallic needles for minimally invasive drug delivery and biofluid extraction [7,8]. These microneedles have the capability to deliver drugs subcutaneously while minimizing the pain inflicted to patients. Recent advancements in

the design and fabrication of hollow metallic microneedles has led to improved fluid handling capabilities, as well as, increased functionality. Recently, McAllister et al. [9] have reported hollow NiFe microneedle arrays.

The paper presents the design, fabrication, and characterization of a hollow metallic active microneedle. Figure 1 is a schematic representation of the described microneedle with an integrated biosensor. The active microneedle includes design features such as tapered needle tips; multiple output ports on the back and front of each needle; multiple lumens and multiple input ports, Figure 2, and bioluminescence based biosensors for monitoring metabolic levels.

## FABRICATION AND PACKAGING

The micromachined multiple output port needles are fabricated using extensions of previously reported micromachining technologies [10,11,12]. The fabrication process is low temperature and is compatible with integrated circuit (IC) technology as a post process. Initially, a metal system of adhesion layers and an electroplating seed layer are electron beam evaporated onto a silicon wafer. Using standard thick photoresist micromolding techniques, this metal layer is patterned and 20µm of palladium is electroplated to form the solid layer or bottom wall of the microneedle [13]. The use of palladium as a structural material provides high mechanical strength and durability, as well as, biocompatibility for use in biomedical applications [14,15,16]. Next, 20µm of commercially available thick photoresist, AZ4620, is deposited and patterned into sacrificial structures. These sacrificial structures serve to precisely define the inner dimension of each microneedle. 800Å of gold is sputter deposited onto the sacrificial photoresist structures to act as an electroplating seed layer for top shell electroplating. Next, a 20µm layer of palladium is electroplated to form the top and side walls (hollow layer) of the microneedle. The sacrificial thick photoresist is then removed

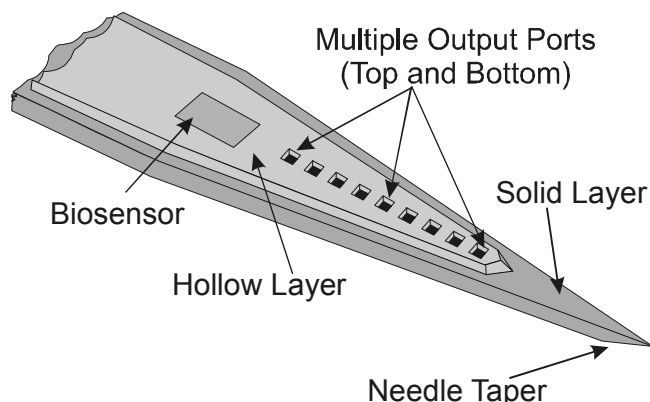


**Figure 1.** Schematic representation of a micromachined multiple output port needle with an integrated biosensor.

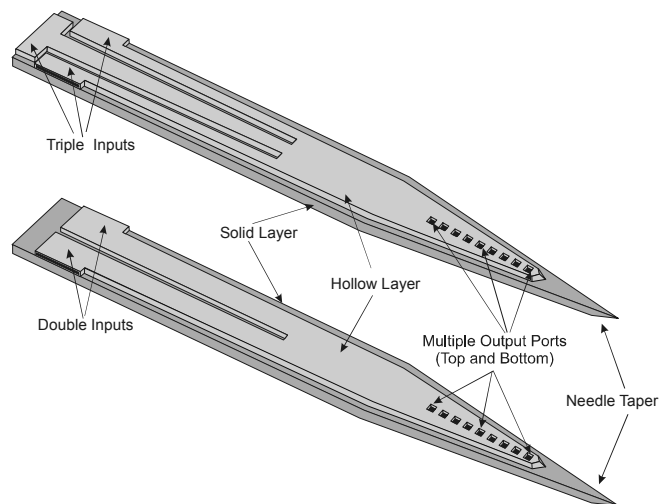


**Figure 2.** Schematic representation of multi-lumen design for the active microneedles.

# ACTIVE MICRONEEDLES WITH INTEGRATED FUNCTIONALITY

JOHN BRAZZLE, DAN BARTHOLOMEUSZ, RUPERT DAVIES, AND JOSEPH ANDRADE

<sup>1</sup>DEPARTMENT OF BIOENGINEERING, UNIVERSITY OF UTAH

SALT LAKE CITY, UTAH 84112

RICHARD A. VAN WAGENEN<sup>1,2</sup>

<sup>2</sup>PROTEIN SOLUTIONS

SALT LAKE CITY, UTAH 84112

A. BRUNO FRAZIER<sup>1,3</sup>

<sup>3</sup>SCHOOL OF ECE, GEORGIA INSTITUTE OF TECHNOLOGY

ATLANTA, GEORGIA 30332

## ABSTRACT

THE FOCUS OF THIS WORK IS THE DESIGN, FABRICATION, AND CHARACTERIZATION OF A NEW CLASS OF BIOMEDICAL MICRO SYSTEMS, THE ACTIVE MICRONEEDLE. ACTIVE MICRONEEDLE SYSTEMS REPRESENT AN ADVANCEMENT OVER CURRENT MICRONEEDLE TECHNOLOGIES THROUGH THE INTEGRATION OF ADDITIONAL FUNCTIONALITY (E.G. BIOCHEMICAL SENSING, MECHANICAL, ETC.). THE ACTIVE MICRONEEDLES DESCRIBED IN THIS PAPER INCLUDE THE FOLLOWING ADDITIONAL FUNCTIONALITY: INTEGRATION OF MULTIPLE INLET/OUTPUT PORTS, MULTIPLE LUMENS (FLOW CHANNELS), AND BIOLUMINESCENCE BASED BIOSENSORS FOR MONITORING METABOLIC LEVELS (E.G. CREATINE AND GLUCOSE).

## INTRODUCTION

BOTH HOLLOW AND SOLID MICRONEEDLES AND MICRONEEDLE ARRAYS HAVE BEEN DEMONSTRATED BY A NUMBER OF RESEARCH GROUPS OVER THE PAST FEW YEARS. INITIALLY, ONLY MICRONEEDLES MADE OF SOLID SILICON HAD BEEN REALIZED [1]. NAJAFI AND WISE DEVELOPED THESE EARLY MICRONEEDLES THAT WERE USED AS NEURAL MICROPROBES. RECENTLY, SOLID SILICON MICRONEEDLES FABRICATED BY HENRY ET. AL. WERE FORMED USING REACTIVE ION ETCHING [2]. THE RESULTING PLANAR NEEDLE ARRAY CONSISTED OF 20x20 NEEDLES FOR INCREASING THE SKIN PERMEABILITY TO DRUGS. LIN, PISANO, AND MULLER WERE FIRST TO PRESENT HOLLOW SILICON PROCESSED MICRONEEDLES [3,4]. THESE MICRONEEDLES WERE FABRICATED ON SILICON SUBSTRATE AND USED SILICON NITRIDE TO FULLY ENCLOSE THE CHANNELS. LATER, CHEN AND WISE [5] PRESENTED HOLLOW SILICON MICRONEEDLES FOR NEURAL RECORDING AND

DRUG DELIVERY. THESE TWO APPROACHES UTILIZE A SACRIFICIAL PROCESSING TECHNIQUE THAT CONSUMES THE SUBSTRATE ON THE DEVICES ARE BUILT. IN CONTRAST, TALBOT AND PISANO [6] HAVE INCORPORATED A POLYSILICON MICROMOLDING PROCESS TO DEVELOP HOLLOW MICRONEEDLES. THESE HOLLOW MICRONEEDLES ARE FABRICATED BY MICROMOLDING POLYSILICON (POLYMOLDING) IN SILICON MICROMOLDS.

PREVIOUSLY, WE REPORTED MICROMACHINED NEEDLES AND NEEDLE ARRAYS OF HOLLOW METALLIC NEEDLES FOR MINIMALLY INVASIVE DRUG DELIVERY AND BIOFLUID EXTRACTION [7,8]. THESE MICRONEEDLES HAVE THE CAPABILITY TO DELIVER DRUGS SUBCUTANEOUSLY WHILE MINIMIZING THE PAIN INFLICTED TO PATIENTS. RECENT ADVANCEMENTS IN THE DESIGN AND FABRICATION OF HOLLOW METALLIC MICRONEEDLES HAS LED TO IMPROVED FLUID HANDLING CAPABILITIES, AS WELL AS, INCREASED FUNCTIONALITY. RECENTLY, MCALLISTER ET AL. [9] HAVE REPORTED HOLLOW NIFE MICRONEEDLE ARRAYS.

THE PAPER PRESENTS THE DESIGN, FABRICATION, AND CHARACTERIZATION OF A HOLLOW METALLIC ACTIVE MICRONEEDLE. FIGURE 1 IS A SCHEMATIC REPRESENTATION OF THE DESCRIBED MICRONEEDLE WITH AN INTEGRATED BIOSENSOR. THE ACTIVE MICRONEEDLE INCLUDES DESIGN FEATURES SUCH AS TAPERED NEEDLE TIPS, MULTIPLE OUTPUT PORTS ON THE BACK AND FRONT OF EACH NEEDLE; MULTIPLE LUMENS AND MULTIPLE INPUT PORTS, FIGURE 2, AND BIOLUMINESCENCE BASED BIOSENSORS FOR MONITORING METABOLIC LEVELS.

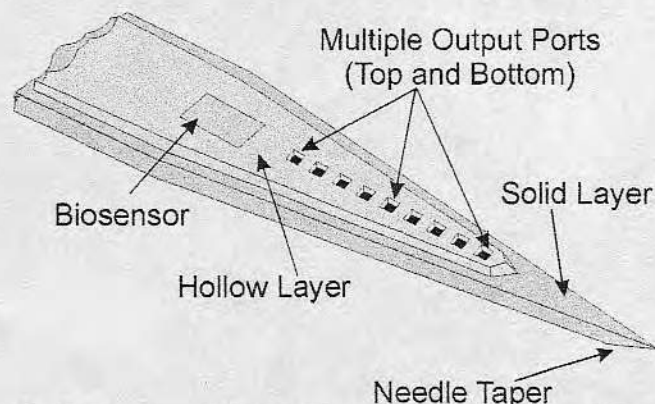


FIGURE 1. SCHEMATIC REPRESENTATION OF A MICROMACHINED MULTIPLE OUTPUT PORT NEEDLE WITH AN INTEGRATED BIOSENSOR.

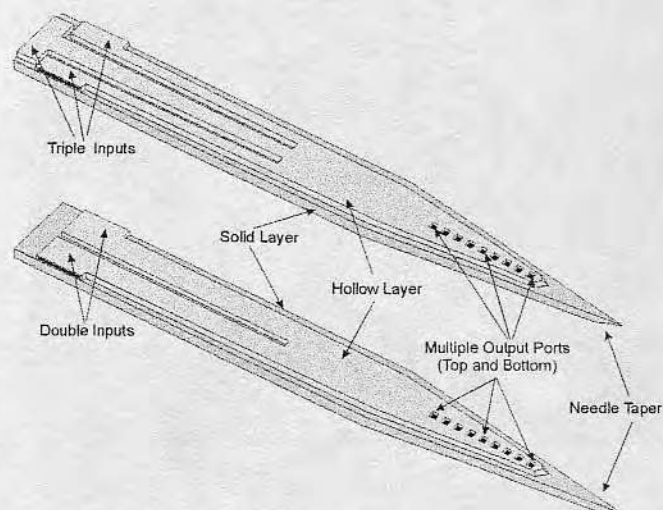
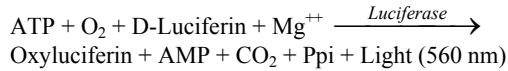


FIGURE 2. SCHEMATIC REPRESENTATION OF MULTI-LUMEN DESIGN FOR THE ACTIVE MICRONEEDLES.

using a sequential rinse in acetone, isopropanol, and de-ionized water, producing the hollow metallic microneedles. In the final step, the microneedles are released from the silicon substrate by first removing the chromium layer to expose the copper seed layer. Then the copper seed layer is etched away from underneath the needles by placing the wafer in a solution of ammonium hydroxide saturated with cupric sulfate. The solid silicon substrate is not consumed in this process and may be re-used. Using the given process offers the flexibility to integrate many additional functions directly onto the microneedle. Additionally, the basic process allows for great latitude in the routing and branching of the fluid

## BIOLUMINESCENCE

Bioluminescence-based analysis is 100 to 1000 times more sensitive than conventional chromogenic (absorbance) measurements and is accurate over a five or more, orders of magnitude concentration range [17]. Firefly bioluminescence occurs by enzyme-catalyzed oxidation of luciferin utilizing adenosine triphosphate (ATP) [18]. Bacteria bioluminescence is closely coupled to nicotinamide adenine dinucleotide hydride (NADH). Since most of biochemistry depends on ATP and/or NADH, nearly all metabolic reactions can be monitored by bioluminescence via one or more enzyme catalyzed and linked reactions [17,18]. During the production or consumption of a metabolite of interest, enzyme linked reactions will cause the production or consumption of ATP (or NADH). Detectable light is then produced via the following reaction (for ATP):



The change in light intensity will be stoichiometrically proportional to the time changing concentration of ATP (and thus proportional to the metabolite of interest). A photodiode or charge-coupled device (CCD) can be used for detection. Depending on the instrument used to detect the luminescence, nanomolar, picomolar, and even femtomolar analyses are possible [17]. With increased sensitivity, smaller amounts of sample fluid are needed for accurate analysis. 0.05- $\mu\text{L}$  sample size that can be drawn by micromachined needles can painlessly access small amounts of body fluid that can be analyzed via bioluminescence.

The transmittance of light through a media across length  $\ell$  is defined by Beer's law,  $T = 10^{-\text{Absorbance}}$ , where  $\text{Absorbance} = \epsilon_{\lambda} C_B (\ell-x)$  and  $\epsilon_{\lambda}$  is the molar absorption coefficient in  $\text{dm}^3/\text{molEcm}$  and  $C_B$  is the concentration in  $\text{mole}/\text{dm}^3$  [19]. If the light is generated within a homogeneous media, the transmitting light is integrated along the length it travels and is then defined as:

$$T_{\text{Total}(\ell)} = \int_0^{\ell} 10^{-\epsilon_{\lambda} C_B (\ell-x)} dx = \frac{(1 - 10^{-\ell})}{\text{Ln}10}$$

where  $\epsilon_{\lambda} C_B$  is assumed to be 1 for simplicity. For a pyramid (which is the shape of the etched wells in the <100> Si wafers) with a peak of length  $\ell$ , the transmittance is integrated through the viewing area and is equal to  $T_{\text{Total}(\ell)} E a^2/3$ . The assumption is that only the light being transmitted toward the viewing window is integrated and light traveling away from the viewing window is absorbed by the substrate. (Light at 560 nm is actually absorbed by crystallized Si). Thus, linear correlation of a volume verses integrated luminosity plot, for a given viewing window, should indicate that transmittance is proportional to signal intensity (averaged CCD counts over the viewing area). A flat bottom well with a reflective surface will have the transmittance of  $T_{\text{Total}(2\ell)}$ , and will be about 2 time larger than  $T_{\text{Total}(\ell)}$  for  $\ell \ll 1\text{-cm}$  (0.005 – 0.025-cm in this experiment). Thus, the slope of a linear fit of volume verses integrated luminosity plot, for a reflective surface of a given viewing window, should be about 2 times that of the slope for a non-reflective surface due to the increased transmittance.

## RESULTS

### Fabrication

The needle arrays fabricated to date include those electroformed from low-stress nickel sulphamate, gold cyanide, and palladium electroplating solutions [20,21]. Individual hollow metallic micromachined needles with multiple output ports fabricated to date have an inner cross-sectional area of  $140 \times 21 \mu\text{m}^2$  (W×H) with outer dimensions of  $200 \times 60 \mu\text{m}^2$ . A micromachined needle fabricated on silicon and released from its substrate is shown in Figure 3. The needle shaft dimensions are 200  $\mu\text{m}$  wide and 60  $\mu\text{m}$  thick while the tip dimensions are less than  $15 \times 15 \mu\text{m}^2$ . The length of the tapered portion of the needle shaft is 1.0 mm and the distance from the tip to the first output port is approximately 300 $\mu\text{m}$ . The total length of the microneedle is 6.0 mm with input port inner dimensions of 140  $\mu\text{m}$  wide and 21  $\mu\text{m}$  high. The wall thickness of the needle is approximately 20  $\mu\text{m}$  and the microneedle output ports are on the top and bottom with dimensions of 30  $\mu\text{m}^2$ . The output ports are separated by 30 $\mu\text{m}$  and there are nine ports on top and 12 ports on the bottom. Bioluminescent detection of the biosensor output is performed at the output ports of the microneedle. Biosensing reagents are drawn into and dried down onto the inner walls of the hollow microneedle.



**Figure 3.** SEM of a multi-lumen, multiple output port micro needle. Shaft dimensions are 200  $\mu\text{m}$  wide and 60  $\mu\text{m}$  thick. Tip dimensions are less than 15  $\mu\text{m}$  X 15  $\mu\text{m}$ . Output ports are 30  $\mu\text{m}^2$ .

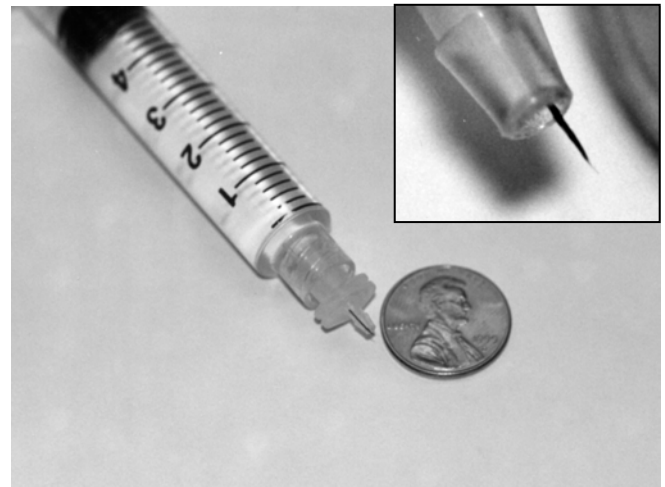


**Figure 4.** Photograph of packaged microneedle connected to standard 5cc syringe as compared to a penny. **Insert:** Close-up of packaged microneedle.



The completed micromachined needle structures were packaged into a standard luer-lock fitting using a polymeric medical-grade UV-curable adhesive (3321, Loctite Corp.). This interface between the microneedle and syringe consists of a simple female luer-to-1/16" barb adapter manufactured by Western Analytical (part# p-857x). Figure 4 is a photograph of a packaged microneedle connected to a standard 5cc syringe as compared to a penny. The insert of Figure 4 shows a close-up of the packaged microneedle that has been secured with UV epoxy on the barbed end of the interface. The UV curable epoxy was found to permanently affix the microneedle to the interface while providing a leak resistant seal. Fluid flow experiments were performed on five packaged microneedles at pressures ranging from 1psi to 70psi [9].

#### Bioluminescence Studies

In order to determine the feasibility and the physical limitations of using bioluminescence as a means for highly sensitive analyte measurement of small sample volumes,  $\mu$ -reaction chambers ( $\mu$ RCs) were fabricated on silicon wafers using KOH anisotropic wet etching. An ATP firefly luciferase/luciferin solution was placed in the  $\mu$ RCs and observed through a close up lens with a CCD. The integrated CCD signal was recorded and compared with well size and depth. The attenuation of the CCD signal was also observed for wafers coated with titanium (500Å) followed by chromium (1500 Å).

A 5-mL firefly luciferase/luciferin solution consisted of 1.25-mg/mL bovine serum albumin (Sigma - reconstituted into the solution. Used for coating the glass vial to prevent denaturing of the luciferase), 1.25-mM ethylene diaminetetra acetic acid (Sigma), 12.5-mM  $Mg^{++}$  (Sigma - from  $MgSO_4$ ), 1.84- $\mu$ M firefly luciferase (Promega), and 1.25-mM luciferin (Biosynth) in a 1.25mM glycyl-glycine buffer. This mixture was able to maintain 90% activity for about 20-hrs when stored in the dark. A 5-mM ATP, glycyl-glycine buffer solution was also prepared. 20- $\mu$ L of the firefly luciferase/luciferin solution was pipetted into 5- $\mu$ L of the ATP solution that resulted in a 1.0-mM ATP mixture, saturated

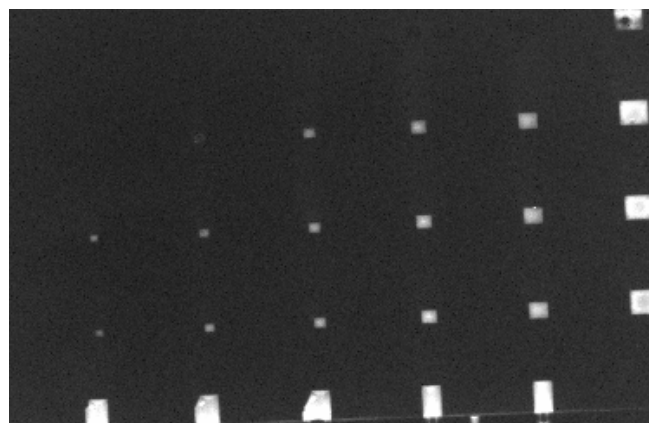


**Figure 5.** 20-sec integration of bioluminescence for the wafer that was etched 242.1- $\mu$ m and coated with Ti/Cr. The  $\mu$ RCs seen here are the 750, 500, 400, 300, 250, and 200- $\mu$ m wide squares.

$\mu$ RC Width ( $\mu$ m)	P value from T-test between Intensity/Volume Slopes of Non-Reflective $\mu$ RCs and Reflective $\mu$ RCs	Ratio of Intensity/Volume Slopes for Reflective and Non-Reflective Substrates
750	<b>0.00001</b>	<b>3.02</b>
500	<b>0.002</b>	<b>2.37</b>
400	<b>0.004</b>	<b>4.94</b>
300	<b>0.005</b>	<b>5.11</b>
250	0.36	2.87
200	0.030	1.07
150	0.72	0.88
100	0.55	0.21

**Table 1.** Statistical comparison of the intensity/volume slope relationships for reflective vs. non-reflective surfaces of the same viewing window size.

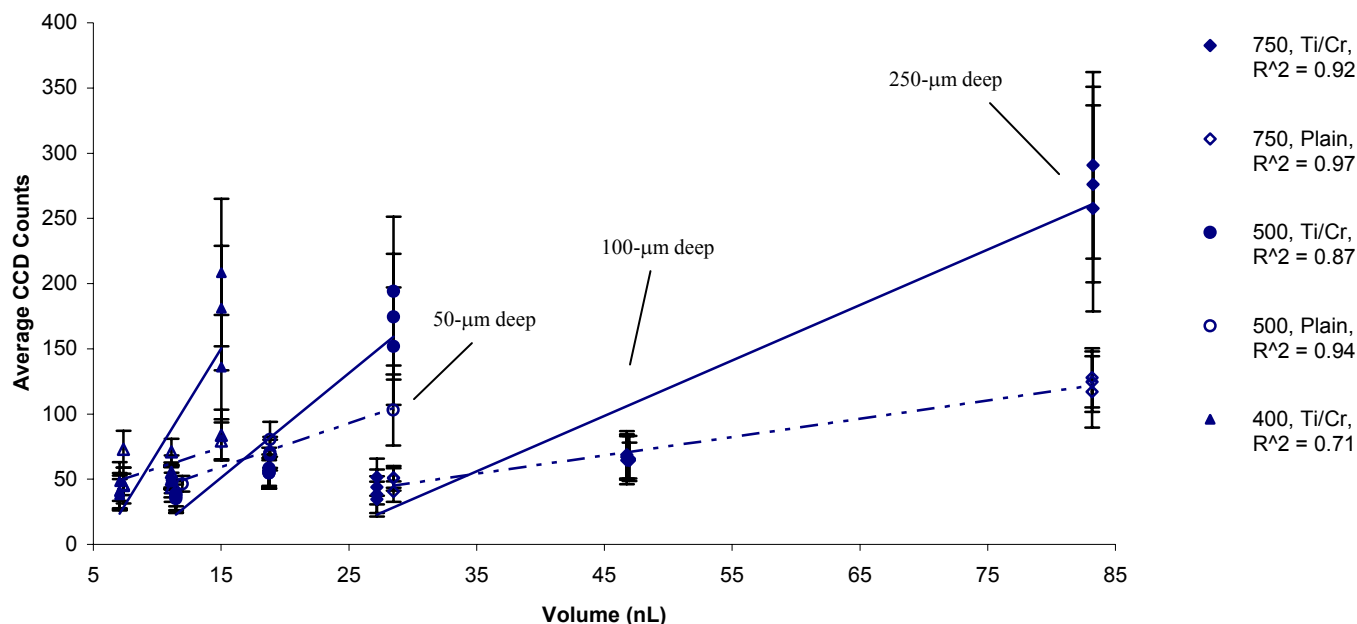


**Figure 6.** Average CCD counts from the 20-sec integrated CCD reading for different sample volumes. Data was plotted in sets for the same viewing area (or  $\mu$ RC square width). Data was also separated according for Ti/Cr reflective substrates and plain, non-reflective, substrates. For each set of data (wells with same width and coating), the increasing volume occurs from the increased etch depths 250- $\mu$ m, 100- $\mu$ m and 50- $\mu$ m. Data from the different etch depths are pointed out for the 750- $\mu$ m wide wells as an example. The higher intensity values occur for the deeper wells. The intensity/volume slope is greater for Ti/Cr reflective substrates than for plain substrates.

with luciferase and luciferin (which means the reaction rate was at it's peak). After the solution mixed, 20- $\mu$ L of it was pipetted on an area about 20 $\times$ 15-mm wide. A thin glass cover slip was placed on the solution, starting at one end and tilting the cover slip as it was laid down, so that the excess bioluminescent fluid would disperse. For high concentrations of ATP ( $> 8\text{-}\mu\text{M}$ ), the initial mixing of ATP with the luciferase/luciferin solution causes a peak luminescence within 3 seconds. The luminescence then tapers and levels off after 1 minute. Therefore, the light measurements for this experiment was integrated for 20 seconds, 2 minutes after the ATP and luciferase/luciferin solution were mixed, with the light intensity essentially constant. An ST6-A CCD camera, by Santa Barbara Instruments Group was fitted with an Olympus wide-angle lens and close-up ring. The experimental substrates were focused 55-mm below the lens with the aperture set at 2.8. The field of view was about 20 $\times$ 15-mm. The camera was operated at  $-20.00^{\circ}\text{C}$ . 1.0-minute after the luciferase/luciferin solution was added to the ATP, a 20-sec dark field exposure was taken with the CCD. 2-min 5-sec after the ATP and luciferase/luciferin solution mixed, the CCD integrated a 20-sec exposure of the bioluminescent reaction while shrouded in a darkroom. The resulting image was saved as a TIF file (Range: 0 – 400). Scion Image (based on the NIH image software) was used to determine the average and standard deviation of the pixel values for each  $\mu$ RC.

Figure 5 shows an image of the 20-second integration of bioluminescence recorded by the CCD camera. One pixel of the CCD image was equal to 46.875- $\mu\text{m}$ . Actual results failed to show light emitting from the 75, 50, 25, and 10- $\mu\text{m}$  wide wells on all substrates. Figure 6 shows the average CCD counts from the 20-sec integrated CCD reading for different sample volumes. Table 1 statistically compares the intensity/volume slope relationships for reflective vs. non-reflective surfaces of the same viewing window size. The reflective wells with intensity/volume slopes that were statistically different from the intensity/volume slopes for the non-reflective surfaces ( $P<0.05$  using the T-test) were over two times greater. This follows the hypothesis that transmittance is nearly doubled for chromium (reflectivity=0.67 @ 560 nm) coated versus uncoated silicon (reflectivity=0.33 @ 560 nm)  $\mu$ RCs.

The intensity/volume slope also increases as the  $\mu$ RC square width decreases. This is ideal for using long, narrow microneedles as the  $\mu$ RC. Table 2 statistically compares the intensity/volume slopes between reflective wells of different viewing widow sizes. It shows that there is a significance increase in the intensity/volumes slopes, as the  $\mu$ RC width decreases. The increase in intensity/volume is only significant down to wells that are 400- $\mu\text{m}$  wide. For smaller  $\mu$ RC widths (150 – 300- $\mu\text{m}$ ), the non-reflective substrates show little correlation between average CCD counts and sample volumes ( $R^2 < 0.25$ ). The Ti/Cr reflective substrates still show some correlation ( $R^2 > 0.25$  for  $\mu$ RCs 250- $\mu\text{m}$  wide and wider) between intensity and volume. However, as the  $\mu$ RC square width decreases (250- $\mu\text{m}$  wide and smaller), there is little difference in signal intensity values for different etch depths.

$\mu$ RC Square Widths Being Compared ( $\mu\text{m}$ )	P value from T-test between Intensity/Volume Slopes $\mu$ RCs being compared	Ratio of Intensity/Volume Slopes for Smaller $\mu$ RC Widths Verses Wider $\mu$ RC Widths
500/750	<b>0.004</b>	<b>1.89</b>
400/500	<b>0.04</b>	<b>1.98</b>
300/400	0.28	1.59
250/300	0.89	1.11
200/250	0.81	1.28
150/200	0.91	0.73

**Table 2.** Statistical comparison of the intensity/volume slopes between reflective wells of different viewing widow sizes. The intensity/volume slope ratio is the slope for the smaller window over the slope for the next larger window.

The error in the signals for wells 200- $\mu\text{m}$  wide and smaller is large enough to overlap with the background intensity. This suggests that the wells with windows smaller than 200- $\mu\text{m}$  wide would not produce signals of a discernable intensity, if they are only 250- $\mu\text{m}$  deep. However, this does not mean that narrower, deeper  $\mu$ RCs like microneedles could not produce a good signal because their longer depths are able to hold a larger sample volume, which would produce a stronger signal according to Beer's Law.

## CONCLUSION

Both silicon and metal electroformed micro needle technologies have been previously developed. This paper provides a basis for the next technological step in micro needle technologies through the development of active micro needles. Active micro needles include the integration of additional functionality into the basic micro needle structure. Additional functionality such as multiple lumens, multiple input and output ports, and the integration of biosensing capabilities has been shown.

## REFERENCES

1. K. Najafi and K.D. Wise, "An implantable multielectrode array with on-chip signal processing," *IEEE J. Solid-State Circuits*, SC-21, pp. 1035-44, Dec. 1986.
2. S. Henry, D.V. McAllister, M.G. Allen, and M.R. Prausnitz, "Micromachined needles for the transdermal delivery of drugs", in *IEEE MEMS Conference*, Heidelberg, Germany, Jan. 25-29, 1998.
3. L. Lin, A.P. Pisano, R.S. Muller, "Silicon processed microneedles," in *Transducers '93', Int.Conf.Solid-State Sensors&Actuators*, pp.237-40, 1993.
4. L. Lin and A.P. Pisano, "Silicon-processed microneedles," in *IEEE J. Microelectromech. Sys.*, vol. 8, no. 1, pp. 78-84, 1999.
5. J. Chen and K.D. Wise, "A multichannel neural probe for selective chemical delivery at the cellular level," in *IEEE Solid-State Sensor & Actuator Workshop*, Hilton Head, SC., June 13-16, pp. 256-259, 1994.
6. N.H. Talbot and A.P. Pisano, "Polymolding: two wafer polysilicon micromolding of closed-flow passages for microneedles and microfluidic devices," in *Tech. Dig. Solid-State Sensor and Actuator Workshop*, Hilton Head, SC., June 8-11, pp. 265-268, 1998.
7. J. Brazzle, I. Papautsky, and A.B. Frazier, "Fluid-coupled metallic microfabricated needle arrays," in *Proc. SPIE Micro Fluidic Devices and Systems*, Santa Clara, CA, Sep. 21-24, pp. 116-124, 1998.
8. J. Brazzle, S. Mohanty, and A.B. Frazier, "Hollow Metallic Micromachined Needles with Multiple Output Ports", *SPIE Micro Fluidic Devices and Systems*, Santa Clara, CA, Sept. 20-21, pp. 257-266, 1999.
9. D.V. McAllister, F. Cros, S.P. Davis, L.M. Matta, M.R. Prausnitz, and M.G. Allen, "Three-dimensional hollow microneedle and microtube arrays," *Transducers '99*, Sendai, Japan, June 7-10, pp. 1098-1101, 1999.
10. I. Papautsky, J. Brazzle, H. Swerdlow, and A.B. Frazier, "A Low Temperature, IC Compatible Process for Fabricating Surface Micromachined Metallic Microchannels", *IEEE Journal of Microelectromechanical Systems*, (7) 267-73 (1998).
11. I. Papautsky, H. Swerdlow, and A.B. Frazier, "Surface Micromachined IC Compatible Technology for Fabricating Metallic MicroChannels", *10th IEEE International Workshop on Micro Electro Mechanical Systems*, Nagoya, Japan, January, 1997, pp. 104-109.
12. J. Brazzle, I. Papautsky, and A.B. Frazier, "Fluid-coupled metallic micromachined needle arrays," in *Proc. 20th International Conference of the IEEE Engineering in Medicine and Biology Society (EMBS '98)*, Hong Kong, Oct. 29 – Nov. 1, pp. 1837-1840, 1998.
13. I. Kadija, V. Chinchankar, V.T. Eckert, E.J. Kudrak, and J. Abys, "Electroplating of thick and ductile palladium: A new electroplating technology," in *Proc. of the 77th Annual Conference of the American Electroplaters and Surface Finishers Society*, July, 1990.
14. J. Black, *Biological performance of materials: Fundamentals of biocompatibility*, Marcel Dekker, New York, 1992.
15. S. D. Cramer and D. Schlain, "Electrodeposition of palladium and platinum from aqueous electrolytes," *Plating*, May, pp. 516-522, 1969.
16. E. J. Kudrak, J. A. Abys, H. K. Straschil, I. Kadija, and J. J. Maisano, "Palladium and palladium alloy plating for the 90's," presented at *Connectors '93*, East Midlands, England, May 19, 1993.
17. S. Brodin and G. Wettermark, *Bioluminescence Anal*, VCH Publ., 1992.
18. A. Campbell, *Chemiluminescence*, VCH Publ., 1989.
20. I.A. Levine, *Physical Chemistry 4<sup>th</sup> ed.*, McGraw-Hill, 1995, pg. 685.

- 
21. W.H. Safranek, *The Properties of Electrodeposited Metals and Alloys*, New York: Elsevier, 1974.
22. J.K. Dennis and T.E. Such, *Nickel and Chromium Plating*, 3rd ed., Cambridge, U.K.:Woodhead, 1993.

## Thermal Analysis of Polymethacrylates and Blends

Lyle R. Brostrom, Dennis L. Coleman, Donald E. Gregonis, Joseph D. Andrade\*

Departments of Bioengineering and Materials Science and Engineering, University of Utah, Salt Lake City, Utah 84112, USA

(Date of receipt: March 12, 1980)

### Introduction

Bulk characterization of poly(alkyl methacrylate)s by thermal analysis is of interest in our investigations of surfaces for biomedical applications. Data available in the literature are incomplete and occasionally contradictory<sup>1)</sup>, possibly due to the plasticizing effect of residual solvent<sup>2)</sup> and to undefined thermal histories. We report thermal transitions of selected methacrylates as a function of casting and curing conditions.

### Experimental Part

Polymers were solvent cast from solutions (1 g/10 ml) into aluminum sample pans. The bulk of the solvent (toluene, methanol, or *N,N*-dimethylformamide) was evaporated from the samples in a few hours. Typically, about 5 mg of dry polymer was contained in each sample pan. Four thermal treatments were selected in order to drive off residual solvent and to produce a defined thermal history: 1) 333 K (60°C) for 3 h; 2) 423 K (150°C) for 2 h; 3) 423 K (150°C) for 2 h followed by slow cooling over 3 h; and 4) 423 K (150°C) for 2 h followed by a liquid N<sub>2</sub> quench after which the specimens were returned to room temperature. Heating occurred under nitrogen and every sample pan was hermetically sealed immediately after being removed from the oven. Thermograms were obtained on a DuPont 990 thermal analyzer and DSC cell base. Glass transitions were determined in the same manner as Russell<sup>3)</sup> and Brennan<sup>4)</sup>. McNaughton and Mortimer<sup>5)</sup> describe the method used for determining melting points. Glass transition data are shown in Tab. 1.

Several of the polymers used were purchased as secondary standards (see Table for source). The remainder were polymerized in our laboratory<sup>6)</sup>. Compositions of copolymers were expressed as the mole fraction of monomer present prior to initiation. Monomer solutions (10 weight-%) containing 1,8 mg dimethyl 2,2'-azodiisobutyrate per ml of monomer, were degassed with argon, heated to 60°C for 24 h, precipitated with a nonsolvent, and dried to constant weight *i.vac.* The glass transition is a function of tacticity in the methacrylates. By C<sup>13</sup> NMR analysis these methacrylate polymers typically exhibit a tacticity of 60% syndio, 40% hetero-, and 0% iso<sup>7)</sup> when radically polymerized at 60°C.

### Discussion

Although poly(*cis*-butadiene) heated to 423 K (150°C) became discolored, the thermal data were comparable to literature values<sup>1)</sup>. The polystyrene-poly(*cis*-butadiene) blend did not discolor at this temperature.

Tab. 1. Observed glass transitions<sup>a)</sup>

Polymers and Copolymers <sup>a)</sup>	Casting solvent	Glass transition temp. in K after thermal pretreatment at				Literature $T_g$ <sup>b)</sup>
		333 K 3 h air cool	423 K 2 h air cool	423 K 2 h slow cool	423 K 2 h N <sub>2</sub> quench	
HEMA	Methanol	329/363	377/377	352/359	374/375	328, 359
MMA <sup>c)</sup>	Toluene	332/368	334/365	347/360	356/358	378
Butyl methacrylate	Toluene	310/312	315/306	314/312	308/352	293
Hexyl methacrylate	Toluene	265/257	262/265	256/—	263/255	268
Octyl methacrylate	Toluene	192/175	211/211	182/192	201/196	203, 253
Dodecyl methacrylate <sup>c)</sup>	Toluene	—	—	—	199/228	208
Octadecyl methacrylate	Toluene	185/179	225/227	—	—	173
75% HEMA/25% MMA	DMF	327/368	365/381	355/384	377/379	—
50% HEMA/50% MMA	DMF	320/332	332/353	358/360	320/345	—
25% HEMA/75% MMA	DMF	359/—	395/356	394/396	397/399	—
3% MAA/97% HEMA	Methanol	348/362	377/376	362/372	403/405	—
3% MAA/97% MMA	Toluene	346/379	349/367	391/375	401/404	—
3% TMAEMA-Cl/97% HEMA	Methanol	354/372	374/383	363/385	363/402	—
3% TMAEMA-Cl/97% MMA	Toluene	349/366	356/373	312/383	359/364	—
Styrene <sup>c)</sup>	Toluene	332/357	340/361	377/379	368/368	373
<i>cis,trans</i> -Butadiene <sup>c)</sup>	Toluene	181/179	183/181	182/182	128/128	269
<i>cis</i> -Butadiene <sup>c)</sup>	Toluene	170/170	168/168	171/171	177/173	171
Blends						
50% MMA <sup>c)</sup> /50% styrene <sup>c)</sup>	Toluene	329/357	378/379	381/382	379/379	—
50% MMA <sup>c)</sup> /50% HEMA	DMF	354/358	379/383	371/377	367/379	—
50% Styrene <sup>c)</sup> /50% <i>cis</i> -butadiene	Toluene	167/167	145/—	170/—	174/169	—
50% Styrene <sup>c)</sup> /50% <i>cis</i> -butadiene	Toluene	227/227	369/369	371/371	371/371	—
50% Styrene <sup>c)</sup> /50% <i>cis</i> -butadiene	Toluene	357/377	—	—	—	—

a) HEMA: hydroxyethyl methacrylate; TMAEMA-Cl: trimethyl-2-methacryloyloxyethylammonium chloride; MMA: methyl methacrylate; MAA: methacrylic acid. Two consecutive thermograms were obtained on each sample. See text for other details.

b) Cf. 1)

c) Purchased as secondary standard (from Aldrich Chemicals). All others were polymerized in our laboratory.

Materials such as poly(hydroxyethyl methacrylate), poly(methyl methacrylate) and polystyrene, with glass transitions near 373 K (100°C), were often plasticized with solvent even after treatment at 423 K (150°C), 30 to 50 K above the glass transition. The escape of solvent from polymer films is discussed by Hansen<sup>8)</sup>.

Polymers and blends of polymers with  $T_g$  much less than room temperature showed only a small variance in  $T_g$  with thermal treatment, presumably because little or no solvent was retained to act as a plasticizer. Poly(dodecyl methacrylate) and poly(octadecyl methacrylate) are very sensitive to changes in thermal history, possibly due to side chain local ordering effects. Duplicate samples of poly(octadecyl methacrylate), heated to 423 K (150°C) for 2 h, prepared simultaneously but thermally analyzed four weeks apart, had marked differences in thermal transitions. Thermograms of the first sample showed no glass transition and an apparent melt at 293 K (20°C). The thermograms of the second sample, after four weeks at 293 K (20°C), showed a glass transition of about 226 K (−47°C) and a melt at 293 K (20°C). A repeat of the second sample five days later gave no apparent  $T_g$  and a melt at 35°C. The temperature range of these thermograms was 93 K (−180°C) to 378 K (+105°C).

The polystyrene-poly(*cis*-butadiene) blend always showed a glass transition near 373 K (100°C) for polystyrene but only twice showed a transition for *cis*-butadiene around 168 K (−105°C). These two polymers form separate domains and do not tend to plasticize one another.

## Conclusion

The glass transition of poly(alkyl methacrylate)s and other polymers may vary by 40 K or more because of residual solvent and thermal history. Some polymers will be affected little by these factors, primarily those with low glass transition temperatures. The results with poly(*cis*-butadiene) and poly(octadecyl methacrylate) document the variability and sensitivity of the glass transition temperature to thermal history and to storage and handling conditions. Care should be used to fully describe a material's solvent and thermal history when reporting glass transition temperatures.

This work was supported by NIH Grant HL 24474-01.

- 1) J. Brandrup, E. H. Immergut, Polymer Handbook, Interscience Publishers, New York 1966
- 2) Y. K. Sung, D. E. Gregonis, G. A. Russell, J. D. Andrade, Polymer 19, 1362 (1978)
- 3) G. A. Russell, Ph. D. Dissertation, University of Utah, Salt Lake City, Utah 1977
- 4) W. P. Brennan, Thermochimica Acta 17, 285 (1976)
- 5) J. L. McNaughton, C. T. Mortimer, "Differential Scanning Calorimetry", in "Physical Chemistry Series, 2", Butterworths, London 1975, Vol. 10
- 6) D. E. Gregonis, C. M. Chen, J. D. Andrade, "Hydrogels for Medical and Related Applications", edited by J. D. Andrade, ACS Symp. Soc. 31, Washington, D.C. 1976, p. 88
- 7) D. E. Gregonis, G. A. Russell, J. D. Andrade, A. C. de Visser, Polymer 19, 1279 (1978)
- 8) C. M. Hansen, Ph. D. Thesis, The Technical University of Denmark, Copenhagen, Danish Technical Press 1967



## Protein Packing in Adsorbed Layers Studied by Excitation Energy Transfer

 E. BRYNDA,\*<sup>1</sup> V. HLADY,<sup>†</sup> AND J. D. ANDRADE<sup>†</sup>

\*Institute of Macromolecular Chemistry, Czechoslovak Academy of Sciences, 162 06 Prague, Czechoslovakia and  
<sup>†</sup>Department of Bioengineering, University of Utah, Salt Lake City, Utah 84112

Received November 13, 1989; accepted March 14, 1990

Excitation energy transfer (EET) from fluorescein donors attached to a bovine serum albumin molecule to tetramethylrhodamine acceptors attached to another albumin molecule in protein assemblies adsorbed on hydrophobized silica was measured by the total internal reflection fluorescence method as a quantity reflecting the arrangement of adsorbed proteins. There was no evidence of albumin aggregation during the growth of albumin-adsorbed layers. Layers obtained by adsorption from mixed albumin and immunoglobulin (IgG) solutions showed a random distribution of the protein molecules on the surface. A higher EET was observed if albumin was adsorbed from 1 mg/ml solution on a clean surface than if the surface was preexposed to low concentrated solutions before the 1 mg/ml solution was applied. The results suggested that at low solution concentrations the surface was saturated with a metastable, less packed albumin layer. © 1990 Academic Press, Inc.

## INTRODUCTION

Protein adsorption is usually discussed in terms of interactions between individual protein molecules and the surface. According to generally accepted models (1) of adsorption a protein molecule usually changes its conformation after contact with the surface so as to achieve a minimum interfacial free energy of the solid surface-adsorbed protein-aqueous solution interface (Fig. 1a). A more realistic picture of the adsorption process should take into account the effects which protein molecules exert on one another. These include simple steric effects, such as insufficient room for an adsorbed protein molecule to realize the full conformation change (Fig. 1c), or protein-protein interactions between adsorbed molecules (Fig. 1d). Globular proteins in solution often aggregate following conformational changes (Fig. 1b). Similarly, a surface-induced conformational change could support the formation of two- or three-dimensional aggregates on the surface.

<sup>1</sup> To whom correspondence should be addressed.

Three examples of adsorbed protein assemblies, in which a surface aggregation could be distinguished, are shown in Fig. 2. In Fig. 2a the surface partly covered with proteins is obtained by stopping the adsorption before a saturation value is reached. When there is a strong protein-protein interaction and the protein solution concentration is high, we expect the adsorbed proteins to be in islands or patches (Fig. 2aB). Individual molecules randomly scattered on the surface are expected if the solution concentration is very low (Fig. 2aA). In Fig. 2B the saturated protein layer contains densely packed regions if formed at a high solution concentration (Fig. 2bB). It is mostly uniform with a larger average area per molecule if adsorbed at low solution concentration (Fig. 2bA). In Fig. 2c the protein layer consisting of two different proteins is obtained by adsorption from a mixed protein solution. Patches of one protein in a matrix of the other protein are expected if a molecule prefers interaction with identical molecules (Fig. 2cB). A random protein mixture is expected if there is no specific interaction (Fig. 2cA).

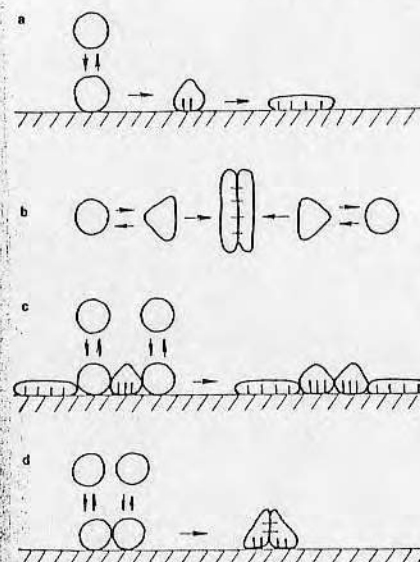


FIG. 1. Protein adsorption at solid-liquid interfaces. (a) Irreversible binding of protein on the surface due to surface-induced conformation change. (b) Aggregation of protein in solutions. (c) An adsorbed molecule does not have enough room to realize the full conformation change because the other molecules are adsorbed in its close vicinity before the conformation change is complete. (d) Aggregation of adsorbed proteins.

Excitation energy transfer has been used for characterization of inter- or intramolecular separations and statistical assemblies of separation distances between donor and acceptor groups in molecular systems (2-4). The high sensitivity of EET to the distance between donor and acceptor groups is suggested by Förster's expression for the rate  $w(r)$  at which an excitation is transferred from an excited donor to an unexcited acceptor a distance  $r$  away (5),

$$w(r) = (1/\tau)(R_0/r)^6, \quad [1]$$

where  $\tau$  is the observed lifetime of the donor excitation and  $R_0$  is the characteristic distance for the donor-acceptor pair for a transfer efficiency of 50%,

$$R_0^6 = 0.88Q_d n^{-4} k^2 J, \quad [2]$$

where  $Q_d$  is the fluorescence quantum yield of the donor,  $n$  is the refractive index of the medium,  $k$  is the orientation factor, and  $J$  is the spectral overlap integral between the donor emission and the acceptor absorption spectra.

For a two-dimensional assembly of donors and acceptors distributed at random, Wobber and Hudson (6) derived an expression for energy transfer quantum efficiency  $f_{da}$  as a function of the number of acceptors,  $n_a R_0^2$ , where  $R_0^2$  is the characteristic area and  $n_a$  is the number of acceptors per unit area.

In the present study the EET from fluorescein label attached to an albumin molecule to tetramethylrhodamine label on another albumin molecule was used for characterization of adsorbed protein assemblies obtained by stopping albumin adsorption before the saturation, by adsorption at various albumin concentrations, and by adsorption from mixed albumin and IgG solutions.

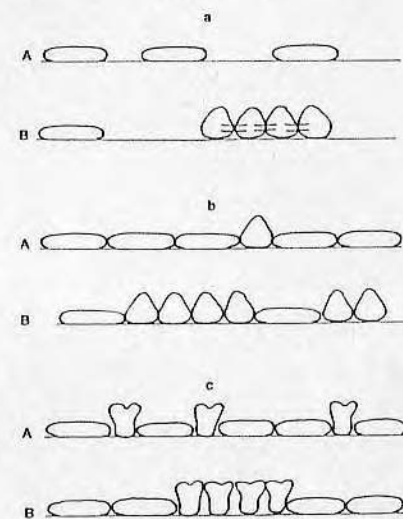


FIG. 2. Examples of adsorbed protein assemblies. (a) Surface partly covered with protein molecules at a low solution concentration (A) and at a high solution concentration if there is protein-protein interaction (B). (b) A saturated protein layer adsorbed at low (A) and high (B) solution concentrations. (c) Layer of a protein mixture if there is no specific interaction (A) or a preferential interaction (B) between molecules of the same kind.

## MATERIALS

Bovine serum albumin (BSA) Fraction V was from Sigma (St. Louis, MO), BSA labeled with 2.3 fluorescein fluorophores per one molecule (BSA-F) and BSA labeled with 5.4 tetramethylrhodamine (TMR) fluorophores per one molecule (BSA-TMR) were from Molecular Probes, Inc. (Junction City, OR), bovine immunoglobulin Fraction II (IgG) was from Miles Laboratories, Inc. (Elkhart, IN). Fluorescein sodium salt, Rhodamine B base, and Eosin Y disodium salt were from Sigma. Physiological buffered solution (phosphate buffer, 0.13 M NaCl) pH 7.4 (PBS) was used for the protein solutions. The substrates for the adsorption were silica slides hydrophobized by the following procedure: The slides cleaned with hot chromosulphuric acid were rinsed in a 0.005 vol% solution of dimethyldichlorosilane (Sigma) in trichloroethylene for 20 min at 23°C, then washed with ethanol and water and baked in an oven at 90°C for 2h.

## METHODS

The concentrations of BSA-F and BSA-TMR solutions were currently measured by the absorbance at 497 nm and 555 nm, respectively. Extinction coefficients of the BSA-F at 497 nm and the BSA-TMR at 555 nm were calculated from the absorbance of a series of solutions in which the protein concentrations were determined by the Bio-Rad (Bio-Rad Laboratories, Berkeley, CA) protein assay method (7). The concentration of BSA and IgG was determined by UV absorption at 280 nm using absorbance values 0.667 and 1.35, respectively, for concentrations of 1 mg/ml. The quantum yield of BSA-F and BSA-TMR in PBS solution was determined using eosin-Y ethanol solution as a standard (8).

The total internal reflection fluorescence (TIRF) of adsorbed proteins was measured in an arrangement described elsewhere (9). The excitation light sources were an argon-ion laser at 477 nm and a green He Ne laser at 543.5 nm, both focused on the same spot on the surface at the same optical geometry using a

semitransparent mirror. The fluorescence intensity  $N$  at the emission wavelength  $\lambda^{em}$  excited by the evanescent electromagnetic field at the surface can be expressed (9)

$$N(\lambda^{em}) = ab(\lambda^{ex})f(\lambda^{em})\Phi\epsilon(\lambda^{ex})\Gamma \times \{1 - \exp[-2\Delta/d_p(\lambda^{ex})]\}, \quad [3]$$

where  $a$  is the fraction of fluorescence collected by the detector,  $b$  is a characteristic of the excitation field,  $\lambda^{ex}$  is the wavelength of excitation light,  $f$  is the fraction of fluorescence emitted at  $\lambda^{em}$ ,  $\Phi$  is the quantum yield,  $\epsilon$  is the extinction coefficient,  $\Gamma$  is the concentration of surface fluorophores,  $\Delta$  is the thickness of the adsorbed layer, and  $d_p$  is the penetration depth of the excitation field. For adsorbed protein layers containing BSA-F and BSA-TMR the ratio  $N_r/N_{tr}$  was measured, where  $N_r$  was the rhodamine emission at 575 nm excited by energy transfer from fluorescein excited at 477 nm and  $N_{tr}$  was the fluorescein emission at 520 nm excited at 477 nm. The emissions were corrected to the spectral sensitivity of the detecting apparatus. Using Eq. [3] one obtains

$$N_r/N_{tr} = [\Phi_r/\Phi_{tr}] \times [f(575 \text{ nm})/f(520 \text{ nm})], \quad [4]$$

where  $\Phi_r$  is the rhodamine quantum yield for excitation via fluorescein and  $\Phi_{tr}$  is the fluorescein quantum yield in the presence of rhodamine.  $f(575)/f(520)$  is constant in all experiments.

From the definition of the energy transfer quantum efficiency  $f_r$  we have

$$f_r/(1 - f_r) = (\Phi_r/\Phi_{tr})(\Phi_f/\Phi_r), \quad [5]$$

where  $\Phi_f$  is the quantum yield of fluorescein emission in the absence of rhodamine and  $\Phi_r$  is the quantum yield of rhodamine emission for direct excitation.

The relation between the measured ratio  $N_r/N_{tr}$  and  $f_r$  is given by expressions [4] and [5]:

$$N_r/N_{tr} = [(1 - f_r)/f_r] \times [f(575 \text{ nm})/f(520 \text{ nm})][\Phi_f/\Phi_r]. \quad [6]$$

$N_r$  was determined from the total emission at 575 nm excited at 477 nm,  $N_{477,575}$ , according to

$$N_r = N_{477,575} - N_{477,r} - N_{477,f}, \quad [7]$$

where  $N_{477,r}$  is the correction for the direct excitation of rhodamine at 477 nm estimated from the rhodamine emission excited at 543.5 nm and the rhodamine fluorescence measured independently in BSA-TMR/BSA-adsorbed layers.  $N_{477,f}$  is the correction for fluorescein emission at 575 nm estimated from emission at 520 nm and from the spectrum of BSA-F/BSA layers. There was no BSA-F emission excited at 543.5 nm and no BSA-TMR emission at 520 nm. No effect of BSA-F in adsorbed mixed layers to the BSA-TMR fluorescence excited at 543.5 nm was assumed. The adsorbed BSA-TMR surface concentration  $c_{BSA-TMR}$  was determined from the TMR fluorescence excited at 543.5 nm using TIRF quantitation according to Hladý *et al.* (9). Series of Rhodamine B or fluorescein solutions at various concentrations excited at 543.5 and 477 nm, respectively, were used to separate the emission excited by the evanescent wave and that excited by the scattered light.

## RESULTS AND DISCUSSION

There was a good overlap of the emission spectrum of BSA-F (maximum at 520 nm) and the absorption band of BSA-TMR (maximum at 518 nm) (Fig. 3a). The quantum yields of BSA-F and BSA-TMR in PBS were 0.29 and 0.022, respectively. The characteristic distance  $R_0 = 4$  nm for EET between the fluorescein label and the TMR label bound on BSA molecules in PBS was calculated from Eq. [2]. No EET was observed in the BSA-F/BSA-TMR solutions used for adsorption experiments. Thus, the absence of BSA-F/BSA-TMR aggregates in solutions could be supposed. The fluorescence spectra of adsorbed BSA-F and BSA-TMR were similar to that measured in PBS solution.

Mixtures of BSA-F/BSA, BSA-TMR/BSA, and BSA-F/BSA-TMR were adsorbed

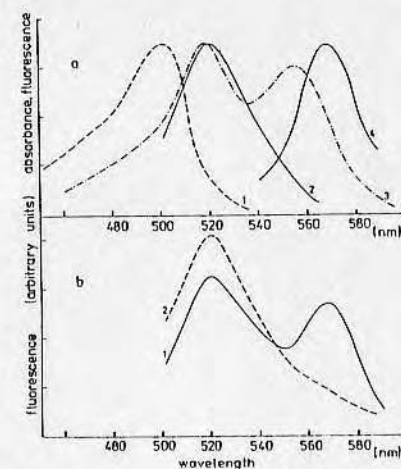


FIG. 3. Absorption and fluorescence emission spectra. (a) Proteins in PBS: (1) BSA-F absorption, (2) BSA-F emission, (3) BSA-TMR absorption, and (4) BSA-TMR emission. (b) Emission spectra excited at 477 nm of saturated protein layers adsorbed on hydrophobic silica: (1) BSA-F/BSA-TMR (2:1) and (2) BSA-F/BSA-TMR/BSA (2:1:12).

on the substrate to test the effect of labeling on BSA adsorption. The total albumin concentration in all solutions was  $10^{-4}$  g/ml. The total albumin concentrations,  $c_p$ , adsorbed on the surface were determined from the fluorescence emission intensity of labeled BSA using TIRF quantitation. The values obtained for saturated adsorbed layers are shown in Table I. The results did not depend on the content of the labeled protein in mixtures up to about 80% of BSA-F and 30% of BSA-TMR, when BSA-F and BSA-TMR emissions were used in the calculation of  $c_p$ , respectively. Thus, there was no preferential adsorption of labeled or native albumin under these conditions. The adsorption kinetics in a BSA-F/BSA (1:2) solution measured by BSA-F emission and in BSA-TMR/BSA (1:2) and BSA-TMR/BSA-F (1:2) solutions measured by BSA-TMR emission were identical. This suggested that labeling did not change kinetics. In a simple BSA-TMR solution the intensity of emission



the adsorbed BSA-TMR increased with time, but after a  $c_p$  of about  $1.2 \cdot 10^{-7} \text{ g cm}^{-2}$  was reached the emission decreased. Similarly, the emission intensity from adsorbed albumin increased with increasing protein concentration in BSA-TMR solution in the same way as in BSA-F solution but after reaching  $c_p = 1.2 \cdot 10^{-7} \text{ g cm}^{-2}$  the emission from adsorbed BSA-TMR decreased with a further increase of BSA-TMR concentration in solution. Both the decrease of BSA-TMR emission in the experiments described above and the apparent decrease of  $c_p$  calculated from BSA-TMR emission at high BSA-TMR content in mixed layers (Table I) could be explained by concentration quenching of TMR fluorescence occurring when distances among adsorbed BSA-TMR molecules became short at high BSA-TMR surface concentrations. The concentration quenching of BSA-TMR fluorescence was probably more effective than that of BSA-F fluorescence due to the larger overlap of absorption and emission spectra of BSA-TMR and the higher degree of TMR labeling. The results obtained under conditions at which the concentration quenching was not effective suggested that BSA, BSA-F, and BSA-TMR behaved in the same way in the

adsorption and that, with the exception of the concentration quenching and EET, the fluorescence quantum yields of BSA-TMR,  $\phi_r$ , and BSA-F,  $\phi_f$ , fluorescence were constant in all adsorbed assemblies.

Mixtures of BSA-F/BSA-TMR (2:1) were used in all EET experiments to eliminate a TMR concentration quenching. The emission peaks of BSA-F at 520 nm and of BSA-TMR at 575 nm could be well distinguished in the fluorescence spectra of adsorbed BSA-F/BSA-TMR layers excited at 477 nm (Fig. 3b). The TMR maximum at 575 nm disappeared if the distance between BSA-F and BSA-TMR in the adsorbed assemblies was increased.

A direct application of EET theory to the protein layers failed for the following reasons: (i) A specific chromophore orientation and a different microenvironment in the adsorbed protein layers could effect the orientation factor  $k$ , the donor and acceptor quantum yields, and the refractive index. Thus, the characteristic distance for EET in adsorbed layers may differ from the  $R_0$  calculated for molecules in solutions. (ii) A complicated pattern of donors on the surface could be formed due to a specific configuration and orientation of fluorophores attached to the albumin molecules.

TABLE I

Saturated Adsorbed Albumin Layers Obtained in Mixed Solutions of BSA-F/BSA, BSA-TMR/BSA, and BSA-TMR/BSA-F

BSA-F/BSA		BSA-TMR/BSA		BSA-TMR/BSA-F	
$n$ % BSA-F	$c_p$ (a) [ $10^{-7} \text{ g cm}^{-2}$ ]	$n$ % BSA-TMR	$c_p$ (b) [ $10^{-7} \text{ g cm}^{-2}$ ]	$n$ % BSA-TMR	$c_p$ (b) [ $10^{-7} \text{ g cm}^{-2}$ ]
10	1.56	10	1.55	10	1.58
		20	1.54		
30	1.61	30	1.57	30	1.56
		40	1.50		
50	1.56	50	1.48	50	1.44
80	1.54	80	1.26	80	1.30
100	1.45	100	1.12	100	1.14

Note. Total labeled and native albumin concentration in solutions was  $10^{-4} \text{ g/ml}$ .  $n$  is the content of the labeled albumin in the mixture in solution and  $c_p$  is the total labeled and native albumin concentration adsorbed on the surface calculated from the emission intensity of (a) adsorbed BSA-F and (b) adsorbed BSA-TMR using TIRF quantitation.

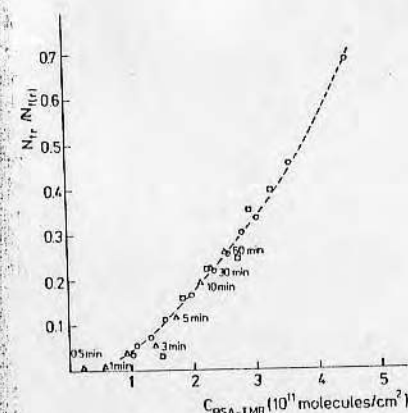


FIG. 4. Fluorescein-TMR energy transfer in the adsorbed layers containing BSA-F/BSA-TMR (2:1). O, adsorbed saturated layers of BSA-F/BSA-TMR diluted with BSA as standard random assemblies. The dashed line was obtained by one curve fitting of the experimental points using polynomial regression.  $\Delta$  1 min, unsaturated adsorbed BSA-F/BSA-TMR assemblies obtained by increasing the time of adsorption at  $10^{-5} \text{ g/ml}$  protein concentration in PBS. The number close to the triangle is the neat contact time of protein solution with the surface.  $\square$ , saturated adsorbed BSA-F/BSA-TMR (2:1) diluted with B1G.

An empirical approach based on the determination of the BSA-TMR surface concentration  $c_{\text{BSA-TMR}}$  and  $N_{\text{fr}}/N_{\text{fr}}$  in the adsorbed protein assemblies was used in this work. As discussed above, quantum yields  $\phi_f$  and  $\phi_r$  were constant in adsorbed albumin layers in which the concentration quenching was negligible. Thus, changes of  $N_{\text{fr}}/N_{\text{fr}}$  were determined only by EET efficiency (see Eq. [6]). The  $c_{\text{TMR}}$  represented a theoretical average distance between albumin molecules if they were considered to be randomly adsorbed on the surface. The actual distances between albumin molecules were reflected by EET efficiency represented by  $N_{\text{fr}}/N_{\text{fr}}$ . A standard dependence of  $N_{\text{fr}}/N_{\text{fr}}$  on  $c_{\text{BSA-TMR}}$  was measured in saturated adsorbed layers obtained by adsorption from solutions prepared by mixing BSA-F/BSA-TMR (2:1) with various amounts of BSA (Fig. 4, open circles). The

total labeled and native albumin concentration in each solution was  $10^{-4} \text{ g/ml}$ . By increasing the BSA content in the adsorbed layers,  $c_{\text{BSA-TMR}}$  was decreased. The obtained experimental data were fitted to an empirical curve by polynomial regression without using EET theoretical expressions. A random distribution of BSA-F and BSA-TMR on the surface was assumed in the adsorbed layers. Any adsorbed protein assembly obtained in the other experiments was characterized by  $c_{\text{BSA-TMR}}$  and  $N_{\text{fr}}/N_{\text{fr}}$ . The latter value was compared with that found for the same  $c_{\text{BSA-TMR}}$  in the standard random BSA-F/BSA-TMR/BSA assembly (dashed line in Figs. 4 and 5). A value  $N_{\text{fr}}/N_{\text{fr}}$  higher than the standard was expected if albumin molecules on the surface were arranged in aggregated structures.

Growth of the adsorbed protein layer was observed by successively interrupting and continuing the adsorption process with PBS and  $10^{-5} \text{ g/ml}$  BSA-F/BSA-TMR solution

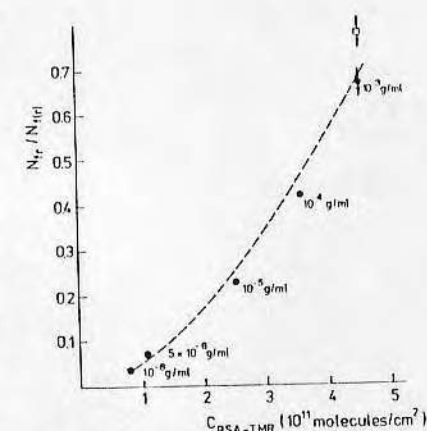


FIG. 5. The formation of BSA-F/BSA-TMR layer by successive increase of the protein concentration in solution from  $10^{-6}$  to  $10^{-3} \text{ g/ml}$  (●) and by direct adsorption at  $10^{-3} \text{ g/ml}$  (□). A point is the energy transfer stationary value obtained after the protein concentration in solution was increased up to the value given below the point. The dashed line is the dependence for the standard random assemblies from Fig. 4. The experimental errors were obtained from five experiments.



(Fig. 4, triangles). The dependence of EET efficiency corresponded to that obtained for a random distribution supposed in standard layers diluted with BSA. Apparently adsorption proceeded by random binding of albumin molecules on surface adsorption sites without observable patchiness (Fig. 2aA). The protein-protein interaction did not significantly affect the adsorption process for the low protein solution concentration case. A stronger protein-protein interaction could be expected at high protein concentrations in solution. However, the adsorption process was too fast to perform a successful stop-flow experiment at high protein concentrations in solution. A similar random distribution of adsorbed protein molecules was obtained by the following experiment: The adsorption started at  $10^{-6}$  g/ml BSA-F/BSA-TMR solution concentration and after the stationary surface concentration was reached, the protein solution was replaced with PBS and EET was measured; subsequently, the procedure was repeated with increasing BSA-F/BSA-TMR solution concentrations  $5 \times 10^{-6}$ ,  $10^{-5}$ ,  $10^{-4}$ , and  $10^{-3}$  g/ml, respectively (Fig. 5). However, if the BSA solution of the highest ( $10^{-3}$  g/ml) concentration was applied directly to the pristine surface, a higher EET efficiency was observed (square in Fig. 5), suggesting a formation of more packed regions of adsorbed albumin molecules on the surface. These results show that when the experiment was finished by exposing the surface to the same highly concentrated solution, the preexposure at lower concentrations formed a metastable, less packed arrangement (Fig. 2bA), which was not changed by further adsorption, while surface protein aggregates were probably formed due to an interprotein interaction (Fig. 2bB) when the protein was adsorbed directly from the concentrated solution.

In order to see whether other protein in the mixture can cause a closer packing of BSA-F and BSA-TMR, experiments were performed by diluting the BSA-F/BSA-TMR (2:1) mixture with B1gG (Fig. 4, squares). The total protein concentration was adjusted to  $10^{-4}$  g/

ml in all solutions. As is evident from Fig. 4 there was no significant difference between the EET dependence obtained by the dilution of BSA-F/BSA-TMR (2:1) with B1gG and the calibration curve obtained by the dilution with BSA. Albumin and B1gG molecules were probably randomly mixed in the adsorbed layers without patching, similar to the arrangement in Fig. 2cA. No evidence of a specific B1gG-B1gG or BSA-BSA interaction was found.

#### CONCLUSION

Protein packing was recognized in only one of the adsorbed molecular assemblies tested here. However, aggregates in adsorbed protein assemblies and protein-protein interactions should be taken into consideration, especially if the proteins are adsorbed at higher concentrations.

#### ACKNOWLEDGMENTS

E. Brynda acknowledges the interinstitutional collaboration between the Institute of Macromolecular Chemistry, Czechoslovak Academy of Sciences, and the Department of Bioengineering, University of Utah, and V. Hladý acknowledges leave of absence from the R. Boskovic Institute, Zagreb, Yugoslavia. This work was partly supported by an NIH grant and an ARO contract.

#### REFERENCES

1. Andrade, J. D., and Hladý, V., *Adv. Polym. Sci.* **76**, 1 (1985).
2. Szollosi, J., Damjanovich, S., Mulhern, S. A., and Tron, L., *Prog. Biophys. Mol. Biol.* **49**, 65 (1987).
3. Estepand, T. N., and Thompson, T. E., *Biophys. J.* **26**, 195 (1979).
4. Lim, C. S., Miller, J. N., and Bridges, J. W., *Anal. Biochem.* **108**, 176 (1980).
5. Birks, J. B., "Photophysics of Aromatic Molecules," p. 567. Wiley-Interscience, New York, 1970.
6. Wobber, P. K., and Hudson, B. S., *Biophys. J.* **28**, 197 (1979).
7. Pollard, H. B., Menard, R., Brandt, H. A., Paróles, C. J., Creutz, C. E., and Ramu, A., *Anal. Biochem.* **86**, 761 (1978).
8. Berlman, I. B., "Handbook of Fluorescence Spectra of Aromatic Molecules," Academic Press, New York, 1971.
9. Hladý, V., Reinecke, D. R., and Andrade, J. D., *J. Colloid Interface Sci.* **111**, 555 (1986).